Contemporary sources dominate carbonaceous aerosol on the North Slope of Alaska

Claire E. Moffett[a], Manisha Mehra[a], Tate E. Barrett[a,b,1], Matthew J. Gunsch[c,2], Kerri A. Pratt[c], and Rebecca J. Sheesley[a,b]

[a]Department of Environmental Science, Baylor University, Waco, TX, USA, [b]The Institute of Ecological, Earth, and Environmental Sciences, Baylor University, Waco, TX, USA, [c]Department of Chemistry, University of Michigan, Ann Arbor, MI, USA, [1]Now at Barrett Environmental, McKinney, TX, USA, [2]Now at Merck & Co., Inc., Kenilworth, NJ, USA

Corresponding author: Rebecca J. Sheesley (Rebecca_Sheesley@baylor.edu; One Bear Place #97266, Waco, TX, 76706-7266)

Contemporary sources dominate carbonaceous aerosol on the North Slope of Alaska

Claire E. Moffett[a], Manisha Mehra[a], Tate E. Barrett[a,b,1], Matthew J. Gunsch[c,2], Kerri A. Pratt[c], and Rebecca J. Sheesley[a,b]

[a]Department of Environmental Science, Baylor University, Waco, TX, USA, [b]The Institute of Ecological, Earth, and Environmental Sciences, Baylor University, Waco, TX, USA, [c]Department of Chemistry, University of Michigan, Ann Arbor, MI, USA, [1]Now at Barrett Environmental, McKinney, TX, USA, [2]Now at Merck & Co., Inc., Kenilworth, NJ, USA

Corresponding author: Rebecca J. Sheesley (Rebecca_Sheesley@baylor.edu; One Bear Place #97266, Waco, TX, 76706-7266)

Highlights

- Influences on organic carbon are regional on the North Slope of Alaska (NSA)
- Influences of elemental carbon are local for an NSA Arctic oilfield
- Biomass burning smoke impacts are episodic on the North Slope of Alaska.
- Contemporary carbon comprises 74% at Utqiaġvik and 63% at an Arctic oilfield.

Abstract

As the Arctic continues to change and warm rapidly, it is increasingly important to understand the organic carbon (OC) contribution to Arctic aerosol. Biogenic sources of primary and secondary OC in the Arctic will be impacted by climate change, including warming temperatures and earlier snow and ice melt. This study focuses on identifying potential sources and regional influences on the seasonal concentration of organic aerosol through analysis of

chemical and isotopic composition. Aerosol samples were collected at two sites on the North Slope of Alaska (Utqiaġvik, UQK, and Oliktok Point, OLK, which is in an Arctic oilfield) over three summers from 2015-2017. The elemental carbon (EC) trends at each site were used to understand local combustion influences. Local sources drove EC concentrations at Oliktok Point, where high EC was attributed to oil and gas extraction activity, including diesel combustion emissions. Utqiaġvik had very low EC in the summer. OC was more similar in concentration and well correlated between the two sites with high contributions of contemporary carbon by radiocarbon apportionment (UQK=74%, OLK=63%), which could include both marine and terrestrial sources of contemporary carbon (e.g. primary and secondary biogenic, biomass burning and/or associated SOA, and bioaerosols). OC concentrations are strongly correlated to maximum ambient temperatures on the NSA during the summer, which may have implications for predicting future OC aerosol concentrations in a warming Arctic. Biomass burning was determined to be an episodic influence at both sites, based on interpretation of combined aerosol composition, air mass trajectories, and remote sensing of smoke plumes. The results from this study overall strongly suggests contribution from regional sources of contemporary organic aerosol on the NSA, but additional analysis is needed to better constrain contributions from both biogenic sources (terrestrial and/or marine) and bioaerosol to better understand temperature-related aerosol processes in the Arctic.

Keywords: Arctic, biomass burning, biogenic secondary organic aerosol, radiocarbon, climate change, organic carbon

1. Introduction

The Arctic is warming at a rate nearly twice as fast as the rest of the planet (Stocker, 2014). Aerosols play a role in the Earth's radiative budget by scattering and absorbing solar radiation and acting as cloud condensation nuclei (CCN) leading to either warming or cooling (Chen and Bond, 2010; Williams et al., 2001). While much Arctic work has focused on aerosol resulting from anthropogenic and marine emissions, specifically black carbon and sulfur aerosol (Breider et al., 2017; Breider et al., 2014; Moffett et al., 2020; Quinn et al., 2009; Sharma et al., 2006; Sharma et al., 2012; Sinha et al., 2017; Winiger et al., 2019), there is increasing interest in organic aerosol sources and processing (Barrett et al., 2015; Becagli et al., 2019; Burkart et al., 2017; Feltracco et al., 2021; Feltracco et al., 2020; Ickes et al., 2020; Kirpes et al., 2018; Leaitch et al., 2018; Moffett et al., 2020). Properly understanding the sources, composition, and concentration of organic aerosol is vital to ensure models are accurately predicting the effects and feedbacks of climate change in the Arctic. However, Arctic aerosol includes a mixture of inorganic and organic components which may vary by season, location and atmospheric processing (Willis et al., 2018). Studying the influence of different sources and controls on organic aerosol is vital to understanding how climate change is affecting the Arctic. A common conclusion among researchers is that the lack of knowledge of natural aerosols currently, will make it more difficult to estimate the presence of natural aerosol in the future as anthropogenic aerosol increases (Leck et al., 2013).

The North Slope of Alaska (NSA) does not always follow the trends in aerosol composition or sources reported for high Arctic locations (Breider et al., 2017; Breider et al., 2014; Quinn et al., 2002; Walker et al., 2005; Winiger et al., 2019). The NSA has two sites Utqiaġvik and Oliktok Point, AK which have had recent field campaigns; Oliktok Point is located within an Arctic oilfield. While aerosol from marine primary production is normally

comparable to other sites with regards to seasonal trends, biomass burning is often over-predicted for Utqiaġvik (Winiger et al., 2019). Breider et al. (2014) noted that the contribution of biomass burning to organic carbon (OC) is often overestimated in the Arctic. Utqiaġvik also does not follow trends of other Arctic sites for sulfate due to its' location close to the Prudhoe Bay oil fields. Within the NSA, Creamean et al. (2018) found that the emissions from oil and gas extraction and exploration activities often remained localized such that Oliktok Point was more impacted than Utqiaġvik. Air masses do travel from Oliktok to Utqiaġvik, however they become diluted during transport (Gunsch et al., 2017). Part of the focus of this study is to determine whether the NSA has a consistent organic aerosol signature, or if the oil and gas activities near Oliktok strongly impact the organic aerosol composition.

Sources of elemental carbon (EC) at Arctic sites, include oil and gas emissions, diesel emissions, gas flaring, and biomass burning (Barrett et al., 2015; Gunsch et al., 2020; Manousakas et al., 2020). For OC, the sources are more complex and can include anthropogenic emissions, fossil fuel combustion, primary biogenic emissions, biomass burning, marine sources, and secondary organic aerosol from organic precursors of all these sources. Several recent studies have reported different trends and sources of organic aerosol in the Arctic. At Cape Baranova, in the Siberian high Arctic, sources of OC include gas flaring, industrial activity, and biomass burning (Manousakas et al., 2020), while results from a cruise through the northern Atlantic and Arctic Ocean indicated that organic aerosol in the open ocean is mainly composed of primary marine emissions (Russell et al., 2010). At Utqiaġvik, Shaw et al. (2010) found organic aerosol in $PM_{1.0}$ was lowest in the summer compared to winter and spring. Barrett et al. (2017) reported that OC concentrations in PM_{10} were similar across seasons at Utqiaġvik in 2012-13, and contemporary sources (e.g. primary and secondary biogenic, biomass burning

and/or associated SOA, and bioaerosols) dominated in spring and summer (69 and 65% contemporary OC, respectively). Moschos et al. (2022) observed that Utqiaġvik and other low latitude Arctic sites had higher contributions from primary and secondary biogenic organic aerosol compared to higher latitude sites in the summer season, when not including organic aerosol associated with methanesulfonic acid (MSA); while high Arctic sites had greater contribution from methanesulfonic acid-associated aerosol, oxygenated organic aerosol, and haze during the winter. Organic aerosol concentrations and sources can be heavily influenced by seasonality, particle size, location, and year-to-year differences; the current study is focused on characterizing trends in contemporary organic aerosol across the NSA considering specifically the influences of local sources, transported biomass burning plumes, secondary biogenic aerosol from marine sources, and local ambient temperature.

The goal of this study is to characterize sources and controls on summertime OC and EC concentrations on the NSA. This study utilizes radiocarbon apportionment, levoglucosan, MSA, aerosol optical properties, and satellite products to determine similarities and differences between the two sites, specifically whether contemporary carbon sources dominate local fossil influences across the NSA.

2. Methods

2.1 Sampling Site and Methods

Total suspended particulate (TSP) matter samples were collected at two sites on the NSA over three years (2015-2017). TSP samples were used to assess aerosol composition which is inclusive of sea spray, dust, combustion and photochemistry-derived aerosol. The sites were Utqiaġvik, AK (formerly Barrow, AK), and Oliktok Point, AK. A detailed description of the sampling sites and methods used can be found in Moffett et al. (2020). Briefly, TSP samples

were collected on quartz fiber filters (QFFs) using high volume samplers (Hi-Q Environmental Products Company, Inc., San Diego, CA). Sample duration was on average 7 days (6.5±1.5 days). Sampling occurred from August-September 2015 and from June 2016-August 2017. In total 37 samples were collected at Utqiaġvik and 42 samples were collected at Oliktok Point during the summertime period. This study focuses on OC and EC analysis of samples collected during the summer periods (June-September). Anion and cation data, including methanesulfonic acid (MSA), has been previously reported for these samples in Moffett et al. (2020).

2.2 Carbon and Isotope Analysis

OC and EC concentrations were determined using a thermal-optical transmittance (TOT) carbon analyzer (Sunset Laboratories, Tigard, OR 97223) using the NIOSH 5040 method (Birch and Cary, 1996). Instrument blanks, field blanks, analytical triplicates, and a sucrose standard were run with each batch of 10 samples. The method detection limit (MDL) was 5.5 ng m^{-3} for OC and 0.37 ng m^{-3} for EC. Field blanks were averaged for each campaign and site and subtracted from the corresponding samples. Field blanks comprised 5.7% and 2.5% of the total carbon at Utqiaġvik and Oliktok Point, respectively, for the 2015 campaign, and 1.9% and 1.4% of the total carbon for the 2016 – 2017 campaign.

For radiocarbon abundance, the sampled filters were cut to provide 100 µg of total organic carbon (TOC) for the ^{14}C measurement. As described in Barrett et al. (2015) the QFFs were placed in prebaked glass Petri-dishes and acidified in a desiccator over hydrochloric acid for 12 hours and then dried in an oven for 1 hour at 60 °C; this acidification process removes any carbonate carbon that would interfere with the radiocarbon analysis. Samples were submitted to the Woods Hole National Oceanic Sciences Accelerator Mass Spectrometry (NOSAMS) facility for analysis. The results are reported as the fraction modern (F_M), or the $^{14}C/^{12}C$ ratio of the

sample compared to the "modern reference," which is 95% of the radiocarbon concentration in 1950 A.D. of NBS Oxalic Acid I (Equation 1).

$$F_M = \frac{(^{14}C\ /^{12}\ C)_{sample}}{(^{14}C\ /^{12}\ C)_{AD_{1950}}} \quad (1)$$

The relative difference between the sample and the reference, F_M, was then corrected for the amount of decay that had taken place between collection and the time of the measurement. This is displayed in Equation 2 where λ is the radiocarbon half-life and the year of sample collection is Y_C. The $\Delta^{14}C$ is calculated from the reported fraction modern using the following established conversion (Stuiver and Polach, 1977):

$$\Delta^{14}C = \left[F_M \times e^{\frac{1}{\lambda}(1950-Y_C)} - 1\right] \times 1000 \quad (2)$$

The $\Delta^{14}C$ was then utilized to apportion the fraction of fossil and contemporary sources on the particles. An end member was defined for both fossil and contemporary. Contemporary carbon includes all primary and secondary organic carbon derived from biomass combustion and biogenic emissions, with an end member value of +107.5‰ ($\Delta^{14}C_{Cont}$), which was based on a 2010 wood burning reference from temperate regions (Barrett et al., 2015; Zotter et al., 2014). Fossil carbon includes organic carbon derived from fossil fuel emissions and combustion; the end member used was -1000‰ ($\Delta^{14}C_{Fossil}$) (Gustafsson et al., 2009). The $\Delta^{14}C$ and end members were then utilized in Equation 3 to calculate the fraction contemporary (f_{cont}) and fraction fossil (1-f_{cont}).

$$\Delta^{14}C_{TOC} = (\Delta^{14}C_{Cont})(f_{Cont}) + (\Delta^{14}C_{Fossil})(1 - f_{Cont}) \quad (3)$$

Field blanks from each campaign and site were prepared in the same manner as samples and submitted to NOSAMS with samples. Blank subtraction was performed on the fraction modern

reported for each sample. Instrumental standard error, blank correction uncertainty, and end-member uncertainty were all included in TOC uncertainty calculations (Yoon et al., 2021).

To better constrain the OC and EC influence on the radiocarbon of TOC, the contemporary carbon for OC was estimated using radiocarbon results for EC for each site from previous studies in 2012 at Utqiaġvik (Barrett and Sheesley, 2017) and in 2016 at Oliktok Point (Gunsch et al., 2020). Assuming the contribution of EC radiocarbon to the TOC radiocarbon abundance is consistent across seasons, the radiocarbon abundance of OC was then calculated (Equation 4). At both sites removing the contemporary carbon due to EC from the percent TOC_{Cont} results in a higher percent OC_{Cont} than percent TOC_{Cont} (Figure S1). TOC_{Cont} includes both OC and EC while OC_{Cont} does not include contributions from EC. At Utqiaġvik this is a 1.4% average increase in the percent OC_{Cont} over the TOC_{Cont}, illustrating that the impact of fossil EC on the TOC at the site is small. At Oliktok Point this increase in the percent OC_{Cont} over the TOC_{Cont} is an average of 5.4%, meaning that the fossil EC sources have a larger impact on the TOC at Oliktok Point.

$$\Delta^{14}C_{OC} = \frac{[TOC]}{[OC]} \times \left(\Delta^{14}C_{TOC} - \left(\frac{[EC]}{[TOC]} \times \Delta^{14}C_{EC} \right) \right) \quad (4)$$

2.3 Testing for Carbonate

To test for possible presence of carbonate, a duplicate filter can be acidified prior to OCEC analysis and compared to the non-acidified OCEC results. As the radiocarbon protocol already includes acidification, the mass of C combusted reported by NOSAMS can be compared to the mass of total carbon (TC) calculated by the TOT carbon analyzer. At both sites 95% of samples were beneath 20% difference between the unacidified and the acidified sample, with only 2 samples at each site being greater than 20% difference. At Utqiaġvik the samples were from 7/6-7/13/2016 and 9/15-9/21/2016. At Oliktok Point the samples were from 8/28-8/31/2016

and 9/29-10/5/2016. To check if this difference was due to the presence of carbonate aliquots of each filter were acidified following the procedure described above and then analyzed on the TOT carbon analyzer. There was no significant difference between the C on the filters before and after acidification meaning there was no carbonate present. The difference between the reported value of carbon from NOSAMS and the TOT analyzer results may be due to discrepancies in the area of the filter sent for radiocarbon analysis, processing differences between the OCEC analysis and NOSAMS, and any contamination during transport.

2.4 Levoglucosan Analysis

Aliquots of the filters were extracted using a previously reported pressurized liquid extraction technique (Clark et al., 2015). Several samples with low OC loadings were composited together in order to ensure enough carbon to analyze via gas chromatography-mass spectrometry (GC-MS) analysis. Composites were calculated so each sample contributed 200 or 300 µg of carbon for a total of 400 or 600 µg of carbon total. A summary of the samples composited together can be found in Table S1. Briefly, each filter or composite was spiked with an isotopically-labeled internal standard and then a Dionex Accelerated Solvent Extractor (ASE) 350 was used to extract the filter samples with a 2:1 v/v dichloromethane:acetone mixture. In order to analyze samples for polar compounds, an aliquot of each extract was derivatized using a silylation method described in Yoon et al. (2021). Briefly, an aliquot of the sample was blown to dryness under a gentle stream of nitrogen. Pyridine and N,O-bis(trimethylsilyl)trifluoroacetamide were added to the vial and it was heated at 70 °C for 1 hour. Samples were immediately analyzed on the GC-MS due to the long-term instability of the silylation products. Levoglucosan was quantified using a five-point calibration curve silylated in the same manner as the samples. The recovery of levoglucosan was determined using a standard

reference material (SRM), Urban Dust 1649b (National Institute of Standards and Technology, Gaithersburg, MD), extracted in the same manner as the samples. The concentration of levoglucosan in the SRM was reported in Louchouarn et al. (2009). The average recovery of levoglucosan was 76±3%. No levoglucosan was detected in the field blanks. The MDL was determined using the average signal to noise ratio within 0.5 min of the levoglucosan peak. The MDL was 0.009 ng m^{-3}. Analysis of additional organic tracers was completed at the same time but will be reported in a future manuscript.

2.5 Auxiliary Analysis

Backward air mass trajectory analysis was completed using the National Oceanic and Atmospheric Administration (NOAA) Hybrid Single-Particle Lagrangian Integrated Trajectory (HYSPLIT) online model for 1 week (Rolph et al., 2017; Stein et al., 2015). Detailed information on the method and results can be found in Moffett et al. (2020). Meteorological data for Utqiaġvik was obtained from the NOAA Earth System Research Laboratory Global Monitoring Laboratory (https://www.esrl.noaa.gov/gmd/obop/brw/). Temperature data for Oliktok Point was obtained from the Atmospheric Radiation Measurement (ARM) Program sponsored by the U.S. Department of Energy (DOE), Office of Science, Office of Biological and Environmental Research, Climate and Environmental Sciences Division (Kyrouac & Holdridge, 2015) (https://doi.org/10.5439/1025220).

The spatial distribution of active fire spots during the sampling period was also studied to determine the location of active fires with the potential to affect the aerosol population at the study sites. The active fire spot data was retrieved from the Visible Infrared Imaging Radiometer Suite (VIIRS), aboard the Suomi-National Polar-orbiting Partnership (S-NPP) satellite (VNP14IDG; 375 m active fire product) (Schroeder et al., 2014). Only the fires with normal and

high confidence levels were used in this study to remove any false fire typically associated with sun glint during daytime. In addition, the NOAA Hazard Mapping System (HMS) Fire and Smoke Analysis product (https://www.ospo.noaa.gov/Products/land/hms.html) was used to identify the presence of smoke over the study sites. The aerosol optical depth (AOD) from MODIS (Moderate Resolution Imaging Spectroradiometer aboard Aqua/Terra) was used to analyze the impact of the active fires on the columnar pollution load. Here the Collection 6.1 (C6.1) Level 3 daily combined dark target and deep blue AOD product retrieved at 550 nm for land and ocean was used (Levy et al., 2013). The MODIS observations from Aqua and Terra were combined to improve spatial coverage of daily AOD. The ability to detect smoke using the NOAA HMS product and AOD retrievals from MODIS can be compromised by cloud cover which limits the ability of the smoke and AOD data to track biomass burning plumes on the NSA.

The Absorption Ångström Exponent (AAE) was calculated for periods identified as having influence from biomass burning events and for the summer average. The AAE was used as a biomass burning indicator as it provides information regarding the presence of smoke at the surface where sampling was occurring. The AAE was calculated as the negative slope of the linear fit of the aerosol absorption coefficient (σ_{abs}) versus the wavelengths on a log-log plot (Moosmüller and Chakrabarty, 2011). Aerosol absorption data was obtained from the ARM data discovery portal (https://adc.arm.gov/discovery/#/). The σ_{abs} measurements were conducted by DOE ARM with a continuous light absorption photometer (CLAP) using the Flynn Algorithm at Utqiaġvik (Shilling and Flynn, 2015) and a particle soot absorption photometer (PSAP) at Oliktok Point (Shilling and Flynn, 2016). The AAE values were calculated using all three

wavelengths: 467 nm, 528 nm, and 652 nm for the CLAP, and 464 nm, 529 nm, and 648 nm for the PSAP.

2.7 Outlier Determination

The interquartile rule was used to identify suspected outliers in the data. The interquartile range was calculated using the third and first quartiles. An upper and lower fence were then calculated using Equation 5a and 5b, where 1.5 is a standard value used to scale the IQR. Any value above the upper fence or below the lower fence was considered a suspected outlier (Hubert & Van der Veeken, 2008).

$$Lower\ fence = Q1 - (1.5 \times IQR) \quad (5a)$$

$$Upper\ fence = Q3 + (1.5 \times IQR) \quad (5b)$$

3. Results and Discussion

3.1 Bulk carbon concentrations and radiocarbon apportionment

Bulk carbon analysis was performed on the summer (June-September) samples from 2015-2017. The average summer concentration of OC was 200±7 ng m^{-3} (avg.±std. dev.) at Utqiaġvik for all three years combined (Table 1). The overall average concentration of EC at Utqiaġvik was 6.0±0.3 ng m^{-3}, which follows previously reported trends of low summer EC concentrations (Breider et al., 2017; Sharma et al., 2006; Sinha et al., 2017). The highest averages over the whole summer for both OC and EC mass concentrations at Utqiaġvik were in 2017, and the lowest were in 2015. At Oliktok Point the average summer concentration of OC was 430±18 ng m^{-3} for all three years combined. For EC the average summer concentration was 43±1 ng m^{-3} at Oliktok Point.

The summers were compared to one another using a paired t test (α=0.05) to evaluate year-to-year variability. For OC the summer of 2015 was significantly different than the summers of 2016 and 2017 for both sites ($p<0.03$). The summers of 2016 and 2017 were not significantly different when considering OC mass concentrations at both sites ($p>0.5$). EC mass concentrations were not significantly different at Utqiaġvik or Oliktok Point ($p>0.05$). Sampling in the summer of 2015 only occurred in August and September, likely impacting the averages for that summer (Table S2), however, the temperatures were also lower during that time period. For more discussion of how this shortened sampling period may have affected the summer averages, please see the Supplementary Materials. All averages were corrected for the sample duration so that shorter samples would not disproportionally affect the result.

Table 1. The average ± standard deviation of weekly concentrations of organic carbon (OC), elemental carbon (EC), OC to EC ratios, levoglucosan, percent TOC_{Cont}, and percent OC_{Cont} for the summer sampling periods. OC, EC, levoglucosan, and percent TOC_{Cont} maximum and minimum are reported with uncertainties. The number of samples are listed in parentheses.

	Utqiaġvik, AK (ng m^{-3})			Oliktok Point, AK (ng m^{-3})		
	2015	2016	2017	2015	2016	2017
OC Avg.	**100 ± 13 (n=8)**	**220 ± 16 (n=16)**	**230 ± 21 (n=13)**	**170 ± 25 (n=7)**	**630 ± 56 (n=20)**	**330 ± 27 (n=15)**
OC Max.	168 ± 26	443 ± 29	571 ± 36	271 ± 21	3330 ± 170	733 ± 44
OC Min.	63 ± 10	82 ± 11	34 ± 9	115 ± 13	98.0 ± 22	44.1 ± 8.5
EC Avg.	**2.8 ± 0.7**	**5.3 ± 0.4**	**8.0 ± 1.2**	**45 ± 8**	**48 ± 3**	**38 ± 3**
EC Max.	13 ± 1	13 ± 1	53 ± 3	86 ± 3.3	239 ± 2.9	132 ± 1.4
EC Min.	<MDL	1.1 ± 0.4	<MDL	3 ± 0.7	<MDL	7 ± 1.0
Levo Avg.	**0.24 ± 0.097 (n=4)**	**1.0 ± 0.1 (n=13)**	**.67 ± .09 (n=12)**	**0.12 ± 0.02 (n=7)**	**1.2 ± 0.1 (n=19)**	**0.33 ± 0.04 (n=14)**
Levo Max.	0.51 ± 0.03	5.2 ± 0.3	3.6 ± 0.2	0.22 ± 0.01	9.6 ± 05	1.63 ± 0.08
Levo Min.	0.030 ± 0.004	0.150 ± 0.007	<MDL	0.060 ± 0.004	<MDL	<MDL

OC:EC Avg.	**14 ± 3**	**42 ± 4**	**34 ± 3**	**9 ± 2**	**13 ± 1**	**11 ± 1**
OC:EC Max.	51.7	134	93.5	42.1	58.1	25.9
OC:EC Min.	9.75	10.6	5.45	2.14	0.81	4.20
% TOC_{Cont} Avg.[a]	**75 ± 25 (n=3)**	**71 ± 5 (n=15)**	**85 ± 8 (n=10)**	**50 ± 7 (n=7)**	**67 ± 4 (n=19)**	**66 ± 8 (n=8)**
% TOC_{Cont} Max.[a]	78 ± 6	90 ± 5	86 ± 6	69 ± 4	90 ± 10	80 ± 5
% TOC_{Cont} Min.[a]	72 ± 7	58 ± 4	66 ±4	29 ± 2	28 ± 3	34 ± 2
% OC_{Cont} Avg.[a]	**77 ± 26**	**73 ± 5**	**87 ± 8**	**55 ± 8**	**73 ± 4**	**70 ± 9**

[a]The n value is not the same for radiocarbon data as not all samples were submitted for analysis.

Ambient concentrations of OC displayed week-to-week variability (Figure 1). OC mass concentrations at the two sites were well correlated (r^2=0.70) indicating regional influences; however, the slope of 1.38 reveals a consistently higher concentration at Oliktok Point (Figure S2). For comparison, OC concentrations were considerably lower than at Fairbanks, AK, which had previously reported TSP OC concentrations of 1,900 ng m^{-3} in the summertime (Haque et al., 2021). Fairbanks is located south of the Brooks Range and experiences both higher urban emissions and more frequent impact from wildfires in the summer (Deshmukh et al., 2018; Deshmukh et al., 2019). The Brooks Range obstructs transport from central Alaska to the NSA (Winiger et al., 2019).

EC ambient concentrations were low during the summer campaigns in Utqiaġvik and Oliktok Point (Table 1 and Figure 1), as expected for the Arctic. However, unlike for OC, the EC concentrations did not correlate well between the sites (r^2=0.20, slope=4.08), indicating the influence of local sources at Oliktok Point which dominate any regional background of EC on the NSA (Figure S2). The EC concentrations were often an order of magnitude higher at Oliktok

Point, likely due to local oil and gas extraction and exploration activity. Gunsch et al. (2020) showed these particles were consistent with diesel combustion. EC concentrations from both sites were low compared to more urban sites such as Fairbanks, AK, where an average TSP EC concentration of 300 ng m^{-3} was reported for the summertime (Haque et al., 2021). The average ratio of OC to EC at Fairbanks was 6.3 (Haque et al., 2021). The OC to EC ratio at Oliktok Point ranged slightly higher than this from 9 to 12. This indicates the influence of local combustion sources including generators and motor vehicles. Utqiaġvik reflected dominance of non-combustion sources with average OC to EC ratios from 13 to 42. High OC:EC ratios indicate that the site has higher influence from contemporary sources such as biogenic emissions and secondary aerosol formation, while lower OC:EC ratios (closer to 1) indicate more influence from fossil fuel combustion (Popovicheva et al., 2019). The low EC concentrations and high OC:EC ratio indicate that there is low regional background and low local influence for EC at Utqiaġvik. During the summer of 2015, Utqiaġvik was influenced by air masses from the oil fields of Oliktok Point for 10% of the study and by the Arctic Ocean for 70% of the study (Gunsch et al., 2017). A previous source apportionment study of EC at Utqiaġvik indicated fossil sources dominate these very low EC summertime averages (Winiger et al., 2019). Analysis of aethalometer-based black carbon (BC) concentrations in a previous campaign at Utqiaġvik revealed no significant difference based on wind sector (Barrett et al., 2015). Utqiaġvik therefore experiences influence from fossil sources via transport. Back trajectory analysis (48 hour) reported previously for Utqiaġvik revealed that 45% of its air masses originated from the Chukchi Sea, the Bering Strait, and west coast of the NSA, 45% from the Beaufort Sea and the east coast of the NSA, and 10% from the interior of Alaska for this campaign period (Moffett et al., 2020). At Oliktok Point air mass influence was comprised of 67% from the Beaufort Sea and

327 east coast of the NSA, 15% from the Chukchi Sea and the west coast of the NSA, and 17% from
328 the interior of Alaska for this campaign period. One-week back trajectories extended further into
329 the Arctic Ocean, extended over the Canadian Arctic Archipelago, or originated in the East
330 Siberian Sea (Moffett et al., 2020). Both sites are therefore likely to be heavily impacted by
331 transport over marine regions, with lesser impacts from other regions and limited transport from
332 North American boreal forested regions.

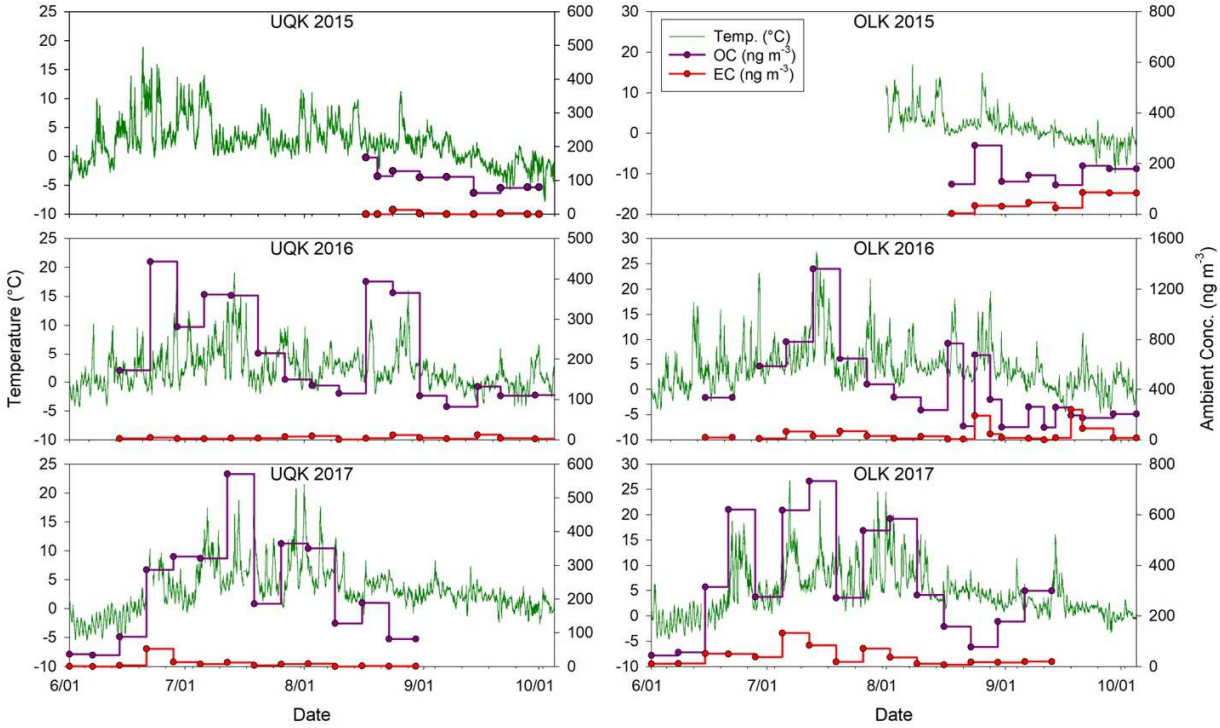

Figure 1. Ambient concentrations of organic carbon (OC, purple) and elemental carbon (EC, red) for both sites (Utqiaġvik=UQK, Oliktok Point=OLK) over the three summers. The temperature is plotted in green behind the OC and EC. The axis scales for both OC and EC as well as temperature are not the same between sites or years.

Radiocarbon source apportionment offers additional insight into the sources influencing TOC at the two sites. The summertime TOC was dominated by contemporary sources at both sites (Figure 2). To determine whether this is driven by contemporary sources such as biogenic (primary or secondary aerosol and/or bioaerosols) or biomass burning sources of TOC, additional source information is needed. As mentioned previously, a recent radiocarbon study of EC has shown that Utqiaġvik has low summertime influence (15%) from biomass burning compared to other Arctic sites and is mainly influenced by fossil sources (Winiger et al., 2019).

Radiocarbon apportionment of EC for Oliktok Point also revealed a dominance of fossil sources (Gunsch et al., 2020). Similarly, single particle analysis showed little influence from biomass burning on Utqiaġvik in 2015 and Oliktok Point in 2016 (Gunsch et al., 2017; Gunsch et al., 2020). OC and EC were not correlated with one another at either site: Utqiaġvik had an r^2=0.26 and Oliktok had an r^2=0.16 (Figure S3). These previous results combined with low regional background of EC on the NSA, indicate a more dominant influence of more biogenic sources of TOC on the NSA. Additional results and discussion of discrete biomass burning events is reported in section 3.2. Overall, there is high influence from contemporary sources to aerosol during the summertime at both sites.

At Utqiaġvik, there was a distinct summer maximum in the contemporary carbon contribution in late summer (i.e. August) for 2016 and 2017 (Figure 2). The percent contribution of contemporary sources was in the 60 – 70% range at the beginning of the summer period (i.e. June) before increasing to 80 – 90% at the end of July to mid-August. The contribution of contemporary carbon then decreased back to the 60 – 70% range at the end of summer and into September. A similar trend appeared at Oliktok Point, except the percent contribution of contemporary sources was lower than Utqiaġvik throughout the season (Table 1) and decreased to the 30 – 40% range in early fall. The total average percent contemporary was 74.2% at Utqiaġvik and 63.0% at Oliktok Point. This trend is repeated across summers despite differences in bulk carbon concentrations. Moschos et al. (2022) determined 68% of aerosol in the summer at Utqiaġvik was from natural sources. This is just slightly lower than the average percent contemporary calculated here. The maximum percent contemporary TOC occurred during the summer of 2016 at both sites with 89.7% at Utqiaġvik and 91.5% at Oliktok Point. At the end of

September 2016, the contemporary contribution increased at both sites. The concentration of OC was small for these samples, so this increase does not reflect a major event.

The average radiocarbon abundances of EC from previous studies at Utqiaġvik (Barrett et al., 2012) and Oliktok Point (Gunsch et al., 2020) were used to understand the contribution from OC and EC to the TOC radiocarbon abundance (see Section 2.2). Although overall the percent OC_{Cont} appears similar between the two sites, it is statistically different (p=0.03), due to the differences in local sources such as oil and gas activity at Oliktok Point. For OC alone, the summer of 2016 had the same average percent contemporary at both sites, while Oliktok Point had more fossil influence in 2015 and 2017 (Table 1).

Both Utqiaġvik and Oliktok Point are dominated by contemporary influence (74% and 63% respectively), which illustrates a strong regional background of biogenic, bioaerosol, and/or biomass burning sources. Levoglucosan can be utilized to determine the impact from biomass burning on the sites; the mass concentrations are plotted below the percent contemporary TOC in Figure 2. The sporadic increases in levoglucosan does not follow the smooth contemporary carbon signal. Even the background levoglucosan appears to peak earlier in the summer than the contemporary carbon. The biomass burning impact on the sites appears to be episodic based on levoglucosan concentrations; however additional data is needed to understand its impact as it can be complicated to fully identify biomass burning events.

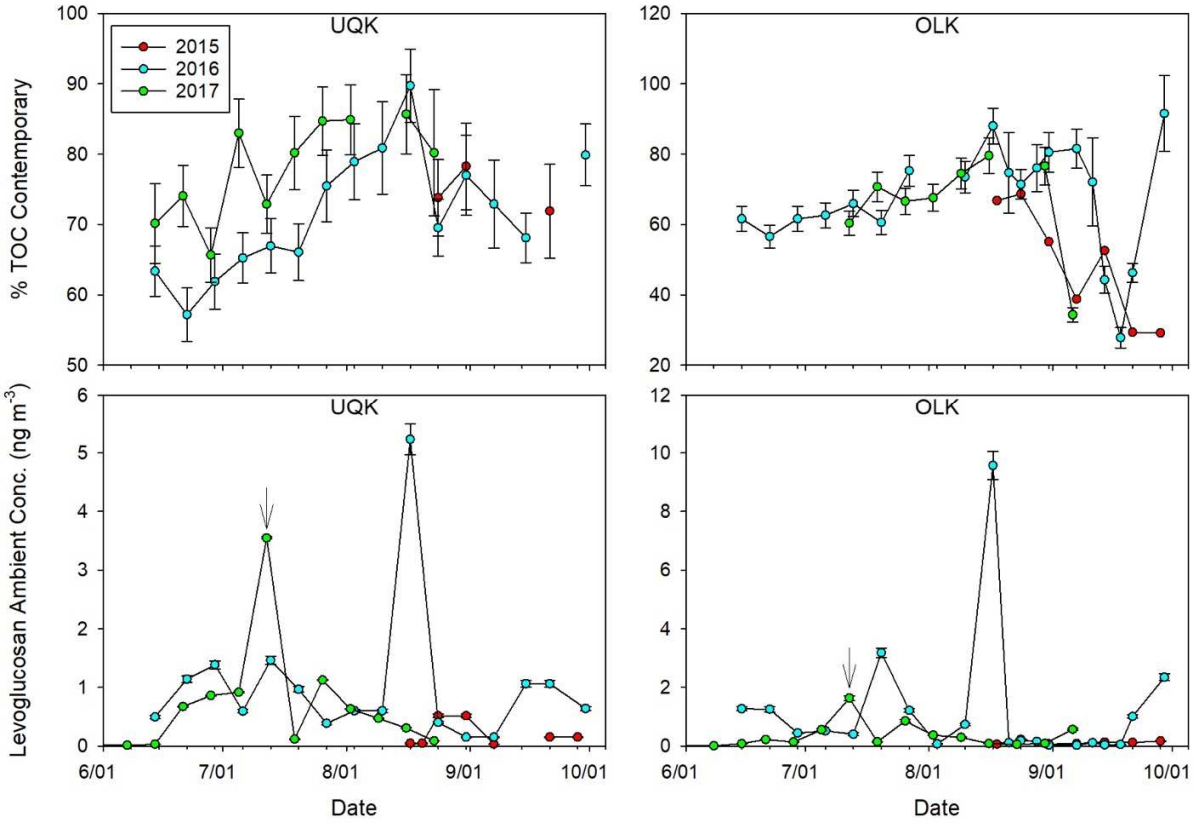

Figure 2. The ^{14}C apportioned total organic carbon (TOC) for contemporary source contribution (top) and ambient concentrations of levoglucosan (bottom) for each site over all sampling years. The arrows on the levoglucosan time series plots indicate the biomass burning event discussed in Section 3.2.

3.2 Biomass Burning Events

Levoglucosan was utilized in this study as a marker for biomass burning impacts on the NSA. Concentrations of levoglucosan were relatively low and consistent at both sites, with a few instances of increased concentrations. Previous research at Utqiaġvik indicated that the half-life of levoglucosan in the atmosphere could range from 20-50 hours for 2-day transit times to 110-290 hours for 5-day transit times in the winter (Barrett et al., 2015). During the summer the half-

lives would be expected to be on the low end of the range due to photodegradation. High concentrations of levoglucosan are therefore not expected at either site as the VIIRS fire data product did not indicate any presence of local fires on the NSA. The average ratio of levoglucosan to OC plus one standard deviation was used as a threshold marker for biomass burning events (UQK=0.006, OLK=0.0035). Four samples at Utqiaġvik and five samples at Oliktok Point were marked as being influenced by biomass burning events (Table 2). The NOAA HMS smoke product, backward air mass trajectories, and VIIRS active fire spot locations were used to verify the possible influence of biomass burning on the sites during the identified biomass burning events (Figure 4). The HMS smoke data was unavailable for the days of interest in 2016, possibly due to high cloud coverage over the NSA (Figure S4). The ground based AAE, which is available for Utqiaġvik in 2016 and for both sites starting in 2017, could be used as confirmation of the presence of smoke at the ground level (Schmeisser et al., 2017). A large amount of data for Utqiaġvik in 2016 and 2017 was unavailable (<40%), resulting in the average AAE of the biomass burning events not displaying an enhancement above the summer average. For the summer of 2017 at Oliktok Point, the majority of data was available (78%), and an enhancement of the AAE for the biomass burning event over the summer average is shown in Table 2. The AOD was mostly unavailable over the sites, likely due to the intense cloud coverage over the NSA (Table 2). Of the biomass burning events, the majority with identifiable source regions originated in the region of Russia/Siberia based on fire spot data combined with back trajectory analysis.

The 7/12-7/19/2017 event is an example of a central Alaska wildfire that does reach the surface stations on the NSA. The backward air mass trajectories combined with VIIRS fire data indicate a potential source region in central Alaska for Utqiaġvik (Figure 4), and the HMS smoke

product has smoke plumes over Utqiaġvik during 7/12-7/15 (Figure S6). The backward air mass trajectories for Oliktok Point during the same period did not indicate air masses passing over the central Alaska fires; however, the smoke data products showed influence from smoke during this period. The Utqiaġvik levoglucosan:OC ratio (Table 2) does show enhancement over the site average, and the levoglucosan concentration is an outlier (using an upper and lower fence) in the 2017 season in Figure 2. Levoglucosan was elevated at Oliktok Point during this period (Figure 2) but was not as high of a concentration as Utqiaġvik. The levoglucosan:OC ratio was also not above the threshold to be considered a biomass burning event for Oliktok Point (Table 2). The average AAE for Oliktok Point during this time period (1.3±0.4) showed an enhancement over the average for the summer of 2017 (1.0±0.4), indicating influence from a biomass burning event (Table 2). The AOD also indicates enhancement over the sites during this time period (Figure S5). The differences between the sites highlights the difficulties in characterizing wildfire influence on the NSA because: 1) it can be difficult to correctly attribute the smoke source, 2) the smoke may remain aloft and surface measurements are needed to confirm if the plume reaches the ground level, 3) organic tracer measurements are impacted by degradation during transport, which complicates assessment of the strength of the source influence (Barrett et al., 2015; Yttri et al., 2011; Hoffmann et al., 2010; Hennigan et al., 2010), 4) long term monitoring data at the surface is not always available. These difficulties in characterizing wildfire influence on the NSA will also make it difficult to identify the impact of biomass burning on OC aerosol.

Table 2. The sample information, levoglucosan concentration, levoglucosan to OC ratio, and information about the fire data product, HMS smoke product, and AAE value for each of the identified biomass burning events. Fire data was available for all samples and the table indicates

445 whether the source region could be identified using that fire data product combined with back
446 trajectories. The column for the biomass burning event described in depth in this section is
447 bolded.

	Utqiaġvik, AK			
Sample Start	8/17/16	9/15/16	9/21/16	**7/12/17**
Sample End	8/24/16	9/21/16	9/30/16	**7/19/17**
Levo Conc. (ng m^{-3})	5.23	0.15	1.06	**3.55**
Levo:OC ratio	0.0133	0.0080	0.0097	**0.0062**
Source Region Identified Using Fire Spot Data	Yes: Russia/Siberia	No	Yes: Russia/Siberia	**Yes: Russia/Siberia, Central Alaska**
HMS Smoke Product Days Available	8/8	7/7	10/10	**7/8**
Number of Days of Smoke Cover	0/8	0/7	0/10	**4/7**
Avg. AAE for Sample Period	0.7 ± 0.4	0.7 ± 0.5	0.7 ± 0.4	**N/A**
Avg. AAE for Summer	0.8 ± 0.4	0.8 ± 0.4	0.8 ± 0.4	**0.79 ± 0.44**
AOD Enhancement	No Data	No Data	No Data	**Yes**

448

	Oliktok Point, AK					
Sample Start	6/15/16	7/20/16	8/17/16	9/21/16	9/29/16	**7/12/17**
Sample End	6/22/16	7/27/16	8/21/16	9/29/16	10/5/16	**7/19/17**
Levo Conc. (ng m^{-3})	1.27	3.18	9.57	1.00	2.34	**1.63**
Levo:OC ratio	0.0038	0.0049	0.0124	0.0058	0.0114	**0.0005**
Source Region Identified Using Fire Spot Data	Yes: Russia/Siberia	No	Yes: Russia/Siberia	Yes: Russia/Siberia, Aleutian Islands	Yes: Russia/Siberia, Alaska	**Yes: Russia/Siberia**
HMS Smoke Product Days Available	8/8	8/8	8/8	9/9	7/7	**7/8**
Number of	0/8	0/8	0/8	0/9	0/7	**6/7**

Days of Smoke Cover						
Avg. AAE for Sample Period	N/A	N/A	N/A	N/A	N/A	**1.3 ± 0.4**
Avg. AAE for Summer	N/A	N/A	N/A	N/A	N/A	**1.0 ± 0.4**
AOD Enhancement	No	No	No	No	No	**Yes**

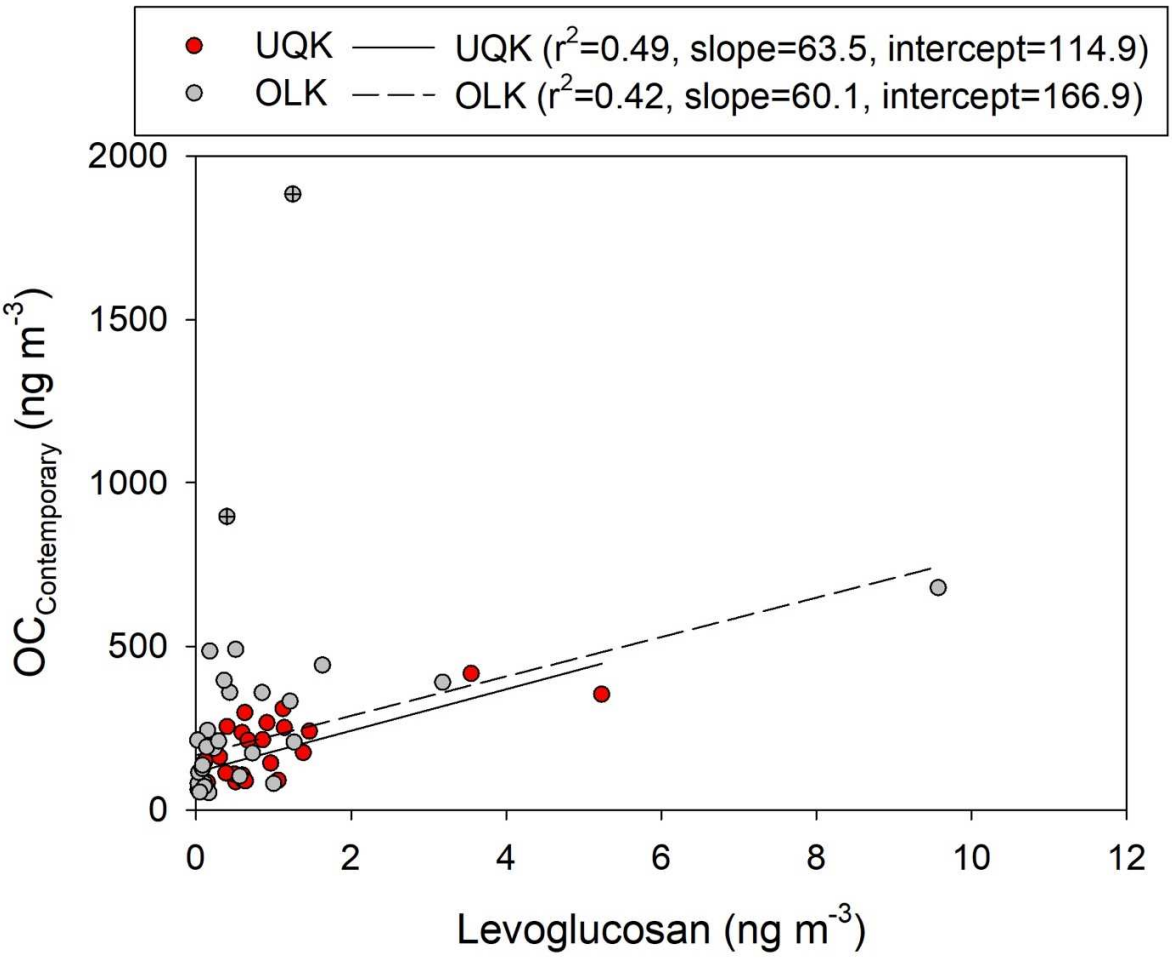

Figure 3. A scatter plot of the ambient concentration of the OC_{Cont} and the ambient concentration of levoglucosan for both sites for all sampling periods. Statistical outliers are marked with a "+", they were calculated using an upper and lower fence.

456

457 The relationship between OC_{Cont} and levoglucosan can be examined to further assess the
458 consistency of the biomass burning influence on OC (Figure 3). The correlation is driven by the
459 few high levoglucosan samples (shown in Figure 3), as lower correlation is evident when these
460 are removed (r^2=0.41 for Utqiaġvik and 0.36 for Oliktok Point). Non-sea-salt potassium (nss-K^+)
461 can also be utilized to understand the influence of biomass burning events, although it has a
462 variety of sources, so it is not a direct measurement. However, no correlation was found between
463 nss-K^+ and levoglucosan or between nss-K^+ and OC_{Cont} for the NSA sites (Figure S7). It is quite
464 possible that coarse aerosol sources of nss-K^+ surrounding the sites make it difficult to identify
465 the small fraction of the total nss-K^+ that results from biomass burning. It is also possible that the
466 lifetime of levoglucosan in the Arctic is too variable to clearly discern a relationship (Barrett et
467 al., 2015), or that differing transport times from fires in different locations results in varying
468 concentrations reaching the site. While there appears to be a consistent low background influence
469 of biomass burning, it is likely not the driving factor of OC concentrations.

470 In summary, the levoglucosan concentrations reported here indicate that biomass burning
471 influence on the NSA during the summer is event-based (during the three summer campaigns:
472 4/37 samples at UQK, 6/42 samples at OLK) with low background concentrations during other
473 time periods. This interpretation matches previous assessments from both modeling and
474 measurement studies. For example, during Sept. 8-30, 2015 at Utqiaġvik, Gunsch et al. (2017)
475 reported that biomass burning from central Alaskan wildfires did not influence the site while
476 biomass burning was a minor contribution (10-14%) to total particles from 0.1-4.0 µm at
477 Utqiaġvik between Aug. 21-Sept. 30, 2015. Single particle mass spectrometry measurements at
478 Oliktok Point from Aug. 22-Sept. 17, 2016, found the average contribution of biomass burning
479 particles between 0.07-1.6 µm was 8% of the particle number concentration (Gunsch et al.,

480 2020). The results of both single particle studies are consistent with the lack of biomass burning
481 transport events identified during these time periods and also consistent with the low
482 levoglucosan:OC ratio observed here (UQK avg. ratio=0.003, OLK avg. ratio=0.001). Stohl et al
483 (2007) and Eck et al (2009) found that Utqiaġvik, AK, was impacted episodically by individual
484 smoke transport events and did not receive constant influence from biomass burning events in
485 spring 2006 and during variable months from 1999-2008 respectively. Breider et al (2017) found
486 similar results of BC being overpredicted at Utqiaġvik because of the overestimation of biomass
487 burning influence using a GEOS-Chem chemical transport model. Utqiaġvik had the lowest
488 fraction biomass burning contribution to summertime EC in a Pan Arctic black carbon study
489 (Winiger et al., 2019). It has been speculated that this is a result of the Brooks Range lofting
490 biomass burning plumes originating in central Alaska to above the boundary layer such that they
491 are only episodically observed at the surface at Utqiaġvik (Quinn et al., 2002; Winiger et al.,
492 2019). Indeed, during our study, the wildfires identified were primarily in Russia/Siberia (Table
493 2). Back trajectory analysis indicates only a small portion of air masses are transported to the site
494 from the interior of Alaska or other North American boreal forests (Moffett et al., 2020). It is
495 possible that very aged biomass burning plumes are being mixed into the contemporary carbon
496 on the NSA, but this influence cannot be tracked via levoglucosan or AAE. As biomass burning
497 influence is only episodic at the site and the radiocarbon abundance indicates contemporary
498 sources, biogenic aerosol and bioaerosols are the other possibility for a contemporary OC source.

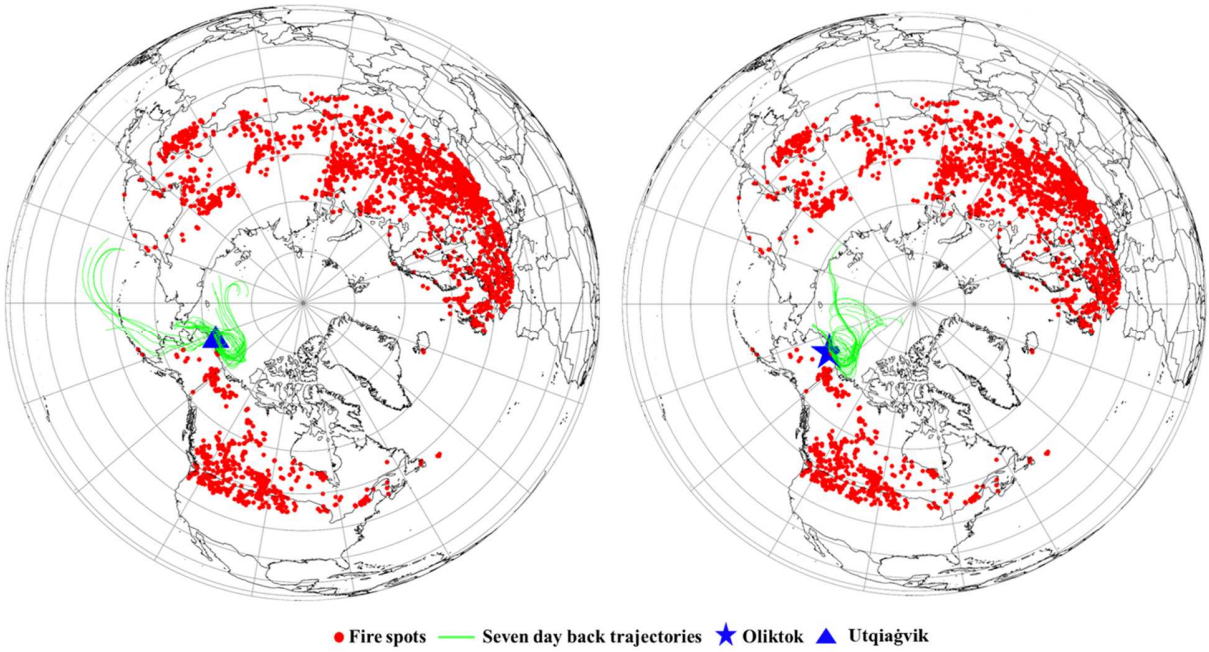

Figure 4. One-week backward air mass trajectories overlaid with satellite retrieved data (VIIRS fire data product) indicating where fire activity occurred during the sample duration from July 12th to July 19th, 2017.

3.3 Relationship between OC and temperature

As the OC is likely comprised of biogenic aerosol and/or bioaerosols, due to the high contemporary and low biomass burning influence, the sources are likely impacted by the environment at the sites. Meteorology in the Alaskan Arctic can vary from year to year. Biogenic sources determine a significant fraction of Arctic aerosol (Section 3.1), and these sources are in turn controlled by the meteorological environment (Bates et al.,1992; Kramshøj et al., 2016; Li et al., 1993; Zhang et al., 2014). In the time series of OC and temperature, there is often an increase in OC concentration when the temperature exceeds 10 °C (Figure 1). The increase in temperature above this threshold may lead to amplified biogenic activity which could cause a corresponding

514 increase in OC ambient concentrations. Recent studies of the impact of increased temperature on
515 biogenic volatile organic compound (BVOC) emissions at Toolik Field Station in Alaska do
516 show exponential increases in emissions of BVOCs above 15-20 °C (Angot et al., 2020).
517 However, an increase in temperature may also indicate the influx of warmer air from the south,
518 bringing biogenic aerosol from other regions. OC mass concentrations and the average maximum
519 temperature of the sample duration (the average of the daily maximums for the sample) are
520 strongly correlated across the summers of 2015-2017 (Figure 5). Individually, Utqiaġvik had an
521 r^2 of 0.71, a slope of 28.7, and an intercept of 42.0 ng m^{-3}, and Oliktok Point had an r^2 of 0.65, a
522 slope of 36.2, and an intercept of 40.6 ng m^{-3}. The intercepts indicate that a similar concentration
523 of carbon at each site is unrelated to temperature. It may have been expected that Oliktok Point
524 would have a higher intercept due to the local oil and gas activity, but this is not apparent in the
525 relationship of the TSP. Oliktok Point has a higher slope here, meaning the OC mass
526 concentration has a strong response to increases in temperature. The summer of 2015 had the
527 lowest average temperatures, much lower max temperatures and the lowest average OC mass
528 concentration (Tables 1 and 3). As the correlations and slopes are similar between sites, it
529 appears that similar sources and/or processes are driving this relationship across the NSA. As
530 mentioned previously, BVOC emissions are expected to increase with temperature, which would
531 be expected to increase the local concentrations of biogenic secondary organic aerosol (SOA).
532 Increased temperature may also impact SOA chemistry and yields; however, there are conflicting
533 processes in play as reduced temperature encourages condensation and partitioning, while
534 increased temperature can change the mechanism or rate of atmospheric reactions (Jonsson et al.,
535 2008; Sheehan and Bowman, 2001; Svendby et al., 2008). In order to further investigate the

impact of secondary biogenic sources on contemporary OC, the relationship with MSA, which is of marine origin, is discussed in the next.

Table 3. The average temperature, maximum temperature, and minimum temperature for all sampling periods at both sites, as well as the r^2 for the linear regression of the average maximum temperature of the sample duration with ambient concentration of OC for each year. Bold type indicates $r^2 > 0.60$.

	Utqiaġvik, AK				Oliktok Point, AK			
Year	Avg. Temp. (°C)	Max. Temp. (°C)	Min. Temp. (°C)	r^2 of OC and Avg. Max. Temp.	Avg. Temp. (°C)	Max. Temp. (°C)	Min. Temp. (°C)	r^2 of OC and Avg. Max. Temp.
2015*	1.37	11.2	-7.8	**0.62**	1.43	16.9	-9.9	0.30
2016	2.27	19.1	-4.3	**0.64**	4.35	27.3	-4.7	**0.61**
2017	3.18	21.5	-5.6	**0.75**	4.69	26.7	-4.6	**0.75**
* Only includes temperature data from August and September 2015								

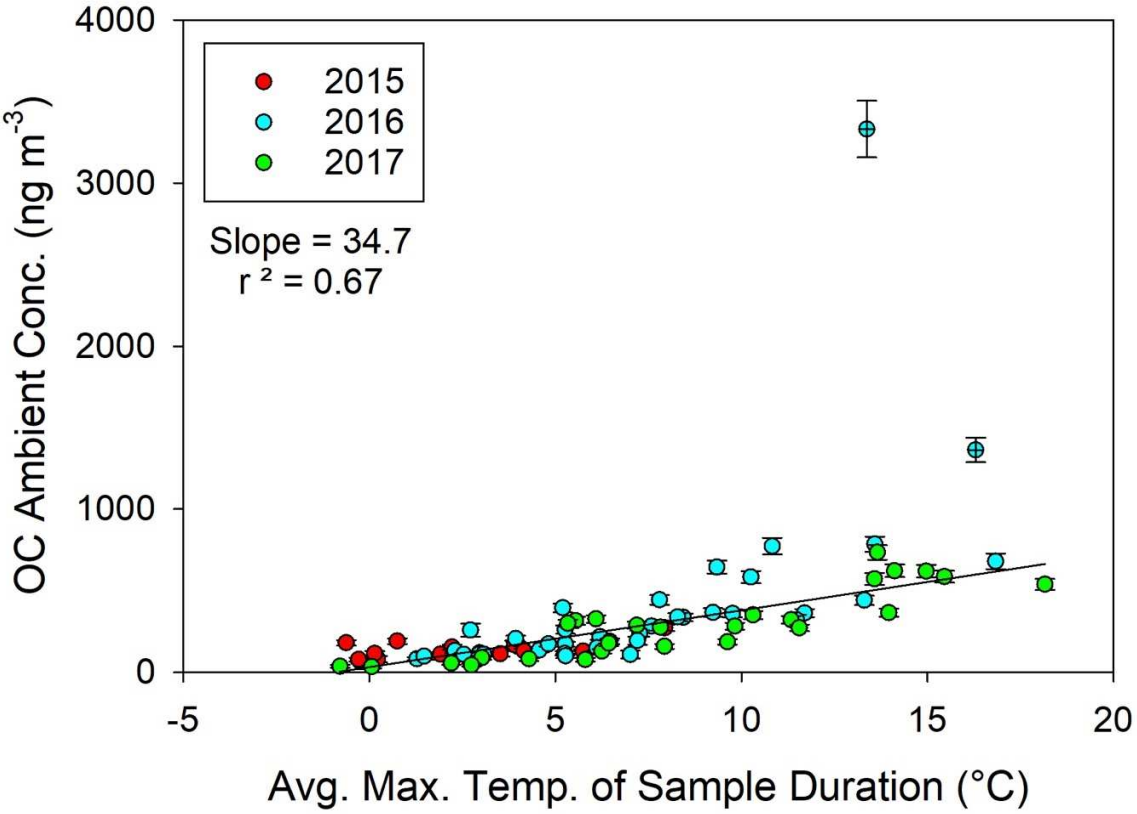

546

547 **Figure 5.** Scatter plots of the ambient concentration of OC and the average maximum
548 temperature of the sample duration at Utqiaġvik and Oliktok Point. Outliers determined
549 statistically are not included in the correlation and are marked with an "+". The two outliers in
550 the summer of 2016 are both from Oliktok Point and are due to local activity.

551

552

553 3.4 Relationship between OC and MSA

554 Previous studies have indicated that marine sources are important for organic aerosol in
555 the Arctic summertime (Moffett et al., 2020; Leaitch et al., 2013). Both sites are influenced
556 heavily by air masses from marine source regions (90% at Utqiaġvik, 82% at Oliktok Point),

with the terrestrial source regions dominated by transport over the NSA (Moffett et al., 2020). MSA is utilized as a proxy for marine influence, although it only reflects marine influence from a single pathway: the photooxidation of dimethyl sulfide released from phytoplankton (Hatakeyama et al., 1985; Leaitch et al., 2013). In order to fully understand the relationship between OC from biogenic sources and MSA, the mass concentration of OC_{Cont} was utilized. There was little difference between the relationship of OC and OC_{Cont} with temperature (OC_{Cont}: r^2=0.63, slope=24.9). Moffett et al. (2020) found that MSA was correlated to temperature (r^2=0.62 at Oliktok Point). Here a relationship between OC_{Cont} and temperature was identified (r^2=0.65 at Oliktok Point), this may indicate a similar temperature dependence for emissions in the Arctic. However, this relationship may be complicated by differences in timescales and reaction mechanisms for OC and MSA. MSA and OC_{Cont} are correlated at Utqiaġvik and Oliktok Point (Figure 5), with an r^2 value of 0.50 and a slope of 6.90 for Utqiaġvik, compared to an r^2 of 0.46 and a slope of 15.3 for Oliktok Point. The correlation is not strong; however, it does point to a need for more comprehensive analysis of the potential marine contribution to OC_{Cont} to better understand how the marine contribution will be impacted by warming Arctic conditions. For example, Moffett et al. (2020) found that MSA, an indicator of marine biogenic activity, correlated highly with average maximum temperature during summers that had intense Arctic cyclone activity at Utqiaġvik from 1998-2017. The summer of 2016 had one such storm, which persisted for over a month beginning in early August, and at one time covered much of the Pacific region of the Arctic Ocean (Yamagami et al., 2017). These cyclones can influence biological activity in the Arctic Ocean (Zhang et al., 2014) and the frequency of their occurrence is likely to increase with melting sea ice. Interestingly, removing data from the summer of 2016 increases the relationship between ambient temperature and OC to an r^2 of 0.74; while the

summer of 2016 has an r^2 of 0.65. These results highlight the complexity of the marine-atmosphere system. The factors influencing MSA concentrations are varied and complicated including ambient temperature, air mass influence region, the occurrence of Arctic cyclones, ocean circulation, and changes in phytoplankton productivity (Moffett et al., 2020). As OC is thought to be impacted heavily by marine sources in the summertime, it likely shares these complicated influencing factors as well as potential temperature dependence for aerosol processes. In addition to marine influence, other sources need to be considered. Both sites receive a small percentage of their air mass influence from terrestrial regions (Moffett et al., 2020). Previous studies have indicated that local inputs of primary biological aerosol particles (PBAPs), such as sugars, increase when the ground is free of snow and ice (Feltracco et al., 2020), which is likely to occur more as the Arctic continues to change. Future work should also focus on identifying the impact of terrestrial contemporary carbon sources on OC, including bioaerosols (e.g. fungal spores, pollen and bacteria).

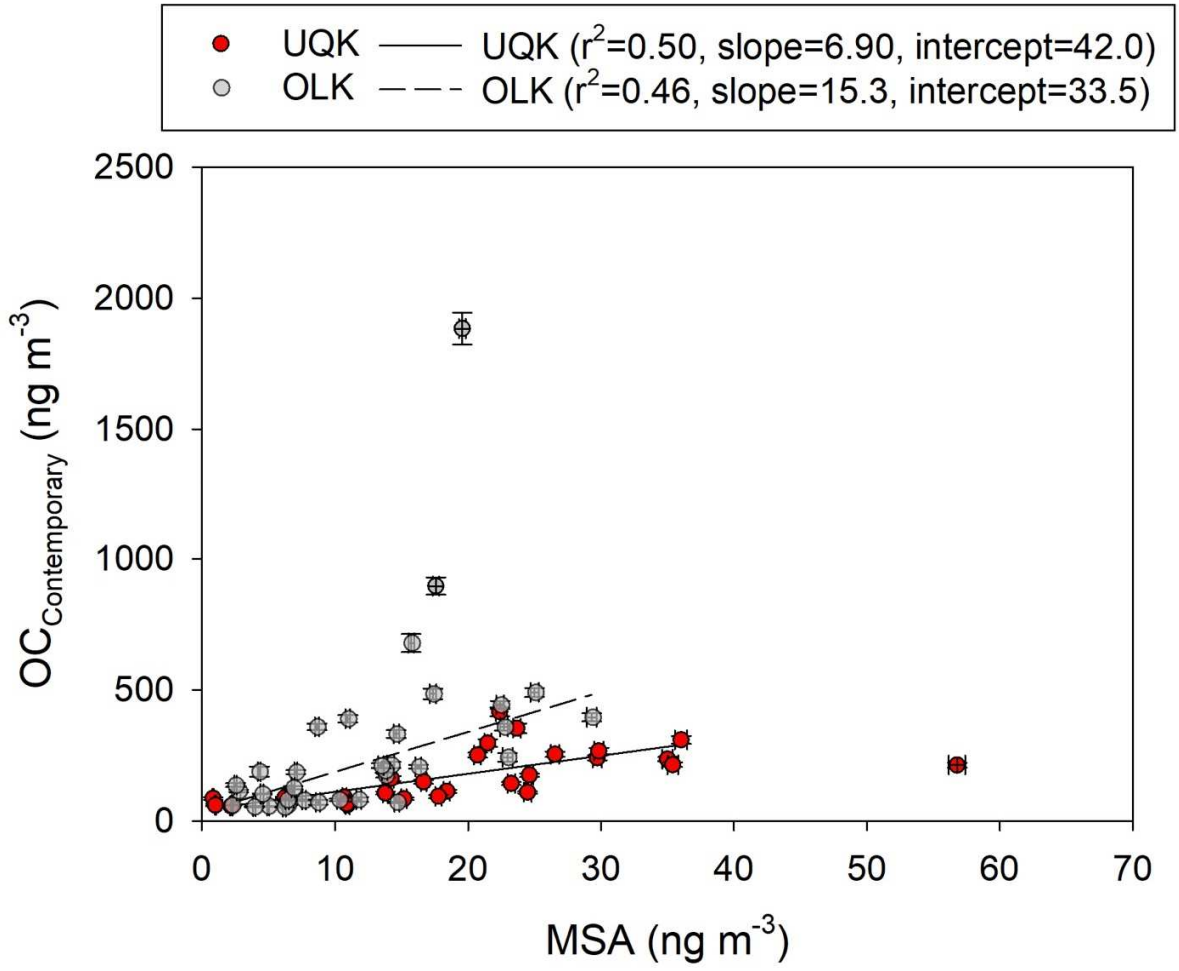

593

594 **Figure 6.** A scatter plot of the ambient concentration of the OC_{Cont} and the ambient
595 concentration of MSA for both sites for all sampling periods. Outliers determined statistically
596 with an upper and lower fence are marked with a "+".

597

598

599 **Conclusions**

600 This study presents a three-summer characterization of OC at two sites on the North
601 Slope of Alaska. Concentrations of EC were low at both sites, but uncorrelated. The influences
602 on EC differed between the two sites with Oliktok Point having local sources and Utqiaġvik
603 mainly dominated by transport. Although, OC concentrations varied over the three summers, the

three-year summer average had a low standard deviation (±6 ng m^{-3} for Utqiaġvik and ±18 ng m^{-3} for Oliktok Point). The OC concentrations at the two sites were well correlated, with highly contemporary radiocarbon signals, strong correlation to ambient temperature and only episodic influence from biomass burning. A weak correlation between OC and levoglucosan signifies that biomass burning is not the driving factor of OC; while the marine influence on summer OC can likely not be fully described based only on the correlation with MSA. The results from this study overall strongly suggest contribution from regional sources of OC aerosol on the NSA, but additional analysis is needed to better constrain contributions from both biogenic sources (e.g. terrestrial vs marine) and bioaerosol to better understand temperature-related aerosol processes in the Arctic.

Acknowledgements

Ambient temperature and aerosol absorption coefficient data was obtained from the Atmospheric Radiation Measurement (ARM) Program sponsored by the U.S. Department of Energy, Office of Science, Office of Biological and Environmental Research, Climate and Environmental Sciences Division. The authors gratefully acknowledge the NOAA Air Resources Laboratory (ARL) for the provision of the HYSPLIT transport and dispersion model and/or READY website (http://www.ready.noaa.gov) used in this publication. Financial and technical support for this campaign was provided by the United States Department of Energy (ARM Field Campaign nos. 2013-6660 and 2014-6694 and Early Career Award no. DE-SC0019172), NOAA (award nos. NA14OAR4310150 and award no. NA14OAR00110149), and the C. Gus Glasscock, Jr. Endowed Fund for Excellence in Environmental Sciences. The authors would also like to thank Walter Brower and Jimmy Ivanoff of the Ukpeaġvik Iñupiat Corporation, and Wessley King,

626 Joshua Remitz, Ben Bishop, and David Oaks for sample collection and field assistance, as well
627 as Fred Helsel, Dan Lucero, and the Sandia National Laboratory for site access and preparation.
628

629 **References**

630 Angot, H., McErlean, K., Hu, L., Millet, D.B., Hueber, J., Cui, K., Moss, J., Wielgasz, C.,
631 Milligan, T., Ketcherside, D., Bret-Harte, M. S., Helmig, D. Biogenic volatile organic
632 compound ambient mixing ratios and emission rates in the Alaskan Arctic tundra.
633 Biogeosciences 2020; 17: 6219-6236. https://doi.org/10.5194/bg-17-6219-2020.
634 Barrett, T.E., Robinson, E., Usenko, S., Sheesley, R.J. Source contributions to wintertime
635 elemental and organic carbon in the western arctic based on radiocarbon and tracer
636 apportionment. Environmental Science & Technology 2015; 49: 11631-11639.
637 https://doi.org/10.1021/acs.est.5b03081.
638 Barrett, T.E., Sheesley, R.J.. Year-round optical properties and source characterization of Arctic
639 organic carbon aerosols on the North Slope Alaska. Journal of Geophysical Research:
640 Atmospheres 2017; 122: 9319-9331. https://doi.org/10.1002/2016JD026194.
641 Bates, T.S., Calhoun, J.A., Quinn, P.K. Variations in the methanesulfonate to sulfate molar ratio
642 in submicrometer marine aerosol particles over the South Pacific Ocean. Journal of
643 Geophysical Research: Atmospheres 1992; 97: 9859-9865.
644 https://doi.org/10.1029/92JD00411.
645 Becagli, S., Amore, A., Caiazzo, L., Iorio, T.D., Sarra, A.d., Lazzara, L., Marchese, C., Meloni,
646 D., Mori, G., Muscari, G., Nuccio, C., Pace, G., Severi, M., Traversi, R. Biogenic
647 Aerosol in the Arctic from Eight Years of MSA Data from Ny Ålesund (Svalbard

Islands) and Thule (Greenland). Atmosphere 2019; 10: 349. https://doi.org/10.3390/atmos10070349.

Birch, M., Cary, R. Elemental carbon-based method for monitoring occupational exposures to particulate diesel exhaust. Aerosol Science and Technology 1996; 25: 221-241. https://doi.org/10.1080/02786829608965393.

Breider, T.J., Mickley, L.J., Jacob, D.J., Ge, C., Wang, J., Sulprizio, M.P., Croft, B., Ridley, D.A., McConnell, J.R., Sharma, S., Husain, L., Dutkiewicz, V.A., Eleftheriadis, K., Skov, H., Hopke, P.K. Multidecadal trends in aerosol radiative forcing over the Arctic: Contribution of changes in anthropogenic aerosol to Arctic warming since 1980. Journal of Geophysical Research: Atmospheres 2017; 122: 3573-3594. https://doi.org/10.1002/2016JD025321.

Breider, T.J., Mickley, L.J., Jacob, D.J., Wang, Q., Fisher, J.A., Chang, R.Y.W., Alexander, B. Annual distributions and sources of Arctic aerosol components, aerosol optical depth, and aerosol absorption. Journal of Geophysical Research: Atmospheres 2014; 119: 4107-4124. https://doi.org/10.1002/2013JD020996.

Burkart, J., Hodshire, A.L., Mungall, E.L., Pierce, J.R., Collins, D.B., Ladino, L.A., Lee, A.K.Y., Irish, V., Wentzell, J.J.B., Liggio, J., Papakyriakou, T., Murphy, J., Abbatt, J. Organic Condensation and Particle Growth to CCN Sizes in the Summertime Marine Arctic Is Driven by Materials More Semivolatile Than at Continental Sites. Geophysical Research Letters 2017; 44: 10725-10734. https://doi.org/10.1002/2017GL075671.

Chen, Y., Bond, T. Light absorption by organic carbon from wood combustion. Atmospheric Chemistry and Physics 2010; 10: 1773-1787. https://doi.org/10.5194/acp-10-1773-2010.

Clark, A.E., Yoon, S., Sheesley, R.J., Usenko, S. Pressurized liquid extraction technique for the analysis of pesticides, PCBs, PBDEs, OPEs, PAHs, alkanes, hopanes, and steranes in atmospheric particulate matter. Chemosphere 2015; 137: 33-44. https://doi.org/10.1016/j.chemosphere.2015.04.051.

Creamean, J.M., Maahn, M., Boer, G.d., McComiskey, A., Sedlacek, A.J., Feng, Y. The influence of local oil exploration and regional wildfires on summer 2015 aerosol over the North Slope of Alaska. Atmospheric Chemistry and Physics 2018; 18: 555-570. https://doi.org/10.5194/acp-18-555-2018.

Creamean, J.M., Hill, T.C.J., DeMott, P.J., Uetake, J., Kreidenweis, S., Douglas, T.A. Thawing permafrost: an overlooked source of seeds for Arctic cloud formation. Environmental Research Letters 2020; 15. https://doi.org/10.1088/1748-9326/ab87d3.

Deshmukh, D.K., Haque, M.M., Kawamura, K., Kim, Y. Dicarboxylic acids, oxocarboxylic acids and α-dicarbonyls in fine aerosols over central Alaska: implications for sources and atmospheric processes. Atmospheric Research 2018; 202: 128-139. https://doi.org/10.1016/j.atmosres.2017.11.003.

Deshmukh, D.K., Haque, M.M., Kim, Y., Kawamura, K. Organic tracers of fine aerosol particles in central Alaska: summertime composition and sources. Atmospheric Chemistry and Physics 2019; 19: 14009-14029. https://doi.org/10.5194/acp-19-14009-2019.

Eck, T., Holben, B., Reid, J., Sinyuk, A., Hyer, E., O'Neill, N., Shaw, G.E., Vande Castle, J.R., Chapin, F.S., Dubovik, O., Smirnov, A., Vermote, S., Schafer, J.S., Giles, D., Slutsker, I., Sorokine, M., Newcomb, W.W. Optical properties of boreal region biomass burning aerosols in central Alaska and seasonal variation of aerosol optical depth at an Arctic

692 coastal site. Journal of Geophysical Research: Atmospheres 2009; 114.
693 https://doi.org/10.1029/2008JD010870.
694 Feltracco, M., Barbaro, E., Spolaor, A., Vecchiato, M., Callegaro, A., Burgay, F., Vardè, M.,
695 Maffezzoli, N., Dallo, F., Scoto, F., Zangrando, R., Barbante, C., Gambaro, A. Year-
696 round measurements of size-segregated low molecular weight organic acids in Arctic
697 aerosol. Science of The Total Environment 2021; 763: 142954.
698 https://doi.org/10.1016/j.scitotenv.2020.142954.
699 Feltracco, M., Barbaro, E., Tedeschi, S., Spolaor, A., Turetta, C., Vecchiato, M., Morabito, E.,
700 Zangrando, R., Barbante, C., Gambaro, A. Interannual variability of sugars in Arctic
701 aerosol: Biomass burning and biogenic inputs. Science of The Total Environment 2020;
702 706: 136089. https://doi.org/10.1016/j.scitotenv.2019.136089.
703 Gunsch, M.J., Kirpes, R.M., Kolesar, K.R., Barrett, T.E., China, S., Sheesley, R.J., Laskin, A.,
704 Wiedensohler, A., Tuch, T., Pratt, K.A. Contributions of transported Prudhoe Bay oil
705 field emissions to the aerosol population in Utqiagvik, Alaska. Atmospheric Chemistry
706 and Physics 2017; 17: 10879-10892. https://doi.org/10.5194/acp-17-10879-2017.
707 Gunsch, M.J., Liu, J., Moffett, C.E., Sheesley, R.J., Wang, N., Zhang, Q., Watson, T.B., Pratt,
708 K.A. Diesel Soot and Amine-Containing Organic Sulfate Aerosols in an Arctic Oil Field.
709 Environmental Science & Technology 2020; 54: 92-101.
710 https://doi.org/10.1021/acs.est.9b04825.
711 Gustafsson, Ö., Kruså, M., Zencak, Z., Sheesley, R.J., Granat, L., Engström, E., Praveen, P.S.,
712 Rao, P.S.P., Leck, C., Rodhe, H. Brown clouds over South Asia: biomass or fossil fuel
713 combustion? Science 2009; 323: 495-498. https://doi.org/10.1126/science.1164857.

714 Hatakeyama, S., Izumi, K., Akimoto, H. Yield of SO2 and formation of aerosol in the photo-
715 oxidation of DMS under atmospheric conditions. Atmospheric Environment (1967) 1985;
716 19: 135-141. https://doi.org/10.1016/0004-6981(85)90144-1.
717 Haque, M.M., Kawamura, K., Deshmukh, D.K., Kunwar, B., Kim, Y. Biomass burning is an
718 important source of organic aerosols in Interior Alaska. Journal of Geophysical Research:
719 Atmospheres 2021; 126. https://doi.org/10.1029/2021JD034586.
720 Hennigan, C.J., Sullivan, A.P., Collett Jr., J.L., Robinson, A.L. Levoglucosan stability in
721 biomass burning particles exposed to hydroxyl radicals. Geophysical Research Letters
722 2010; 37. https://doi.org/10.1029/2010GL043088.
723 Hoffmann, D., Tilgner, A., Iinuma, Y., Herrmann, H. Atmospheric stability of levoglucosan: a
724 detailed laboratory and modeling study. Environmental Science & Technology 2010; 44:
725 694-699. https://doi.org/10.1021/es902476f.
726 Hubert, M., Van der Veeken, S. Outlier detection for skewed data. Journal of Chemometrics
727 2008; 22: 235-246. https://doi.org/10.1002.cem.1123.
728 Ickes, L., Porter, G.C., Wagner, R., Adams, M.P., Bierbauer, S., Bertram, A.K., Bilde, M.,
729 Christiansen, S., Ekman, A.M.L., Gorokhova, E., Höhler, K., Kiselev, A.A., Leck, C.,
730 Möhler, O., Murray, B.J., Schiebel, T., Ullrich, R., Salter, M. The ice-nucleating activity
731 of Arctic sea surface microlayer samples and marine algal cultures. Atmospheric
732 Chemistry and Physics 2020; 20: 11089-11117. https://doi.org/10.5194/acp-20-11089-
733 2020.
734 Jonsson, Å.M., Hallquist, M., Ljungström, E. The effect of temperature and water on secondary
735 organic aerosol formation from ozonolysis of limonene, Δ^3-carene and α-pinene.

736 Atmospheric Chemistry and Physics 2008; 8: 6541-6549. https://doi.org/10.5194/acp-8-
737 6541-2008.
738 Kirpes, R.M., Bondy, A.L., Bonanno, D., Moffet, R.C., Wang, B.B., Laskin, A., Ault, A.P.,
739 Pratt, K.A. Secondary sulfate is internally mixed with sea spray aerosol and organic
740 aerosol in the winter Arctic. Atmospheric Chemistry and Physics 2018; 18: 3937-3949.
741 https://doi.org/10.5194/acp-18-3937-2018.
742 Kramshøj, M., Vedel-Petersen, I., Schollert, M., Rinnan, Å., Nymand, J., Ro-Poulsen, H.,
743 Rinnan, R. Large increases in Arctic biogenic volatile emissions are a direct effect of
744 warming. Nature Geoscience 2016; 9: 349-352. https://doi.org/10.1038/ngeo2692.
745 Kyrouac, J., Holdridge, D. Surface Meteorological Instrumentation (MET), ARM Data Center,
746 2015, updated hourly. Aug. 2015-Oct. 2015, Jun. 2016-Oct. 2016, Jun. 2017-Oct. 2017.
747 ARM Mobile Facility (OLI) Oliktok Point, Alaska, AMF3 (M1). Atmospheric Radiation
748 Measurement (ARM) user facility Data Center: Oak Ridge, Tennessee, USA. Data set
749 accessed 2018-04-03 at http://www.archive.arm.gov/discovery/#v/results/s/fdsc::met.
750 https://doi.org/10.5439.1025220.
751 Leaitch, W.R., Russell, L.M., Liu, J., Kolonjari, F., Toom, D., Huang, L., Sharma, S.,
752 Chivulescu, A., Veber, D., Zhang, W. Organic functional groups in the submicron aerosol
753 at 82.5 degrees N, 62.5 degrees W from 2012 to 2014. Atmospheric Chemistry and
754 Physics 2018; 18: 3269-3287. https://doi.org/10.5194/acp-18-3269-2018.
755 Leaitch, W.R., Sharma, S., Huang, L., Toom-Sauntry, D., Chivulescu, A., Macdonald, A.M.,
756 Salzen, K.v., Pierce, J.R., Bertram, A.K., Schroder, J.C., Shantz, N.C., Chang, R.Y.W.,
757 Norman, A-L. Dimethyl sulfide control of the clean summertime Arctic aerosol and

758 cloud. Elementa: Science of the Anthropocene 2013; 1.
759 https://doi.org/10.12952/journal.elementa.000017.
760 Levy, R.C., Mattoo, S., Munchak, L.A., Remer, L.A., Sayer, A.M., Patadia, F., Hsu, N.C. The
761 Collection of 6 MODIS aerosol products over land and ocean. Atmospheric Measurement
762 Techniques 2013; 6, 2989-3034. https://doi.org/10.5194/amt-6-2989-2013.
763 Li, S.M., Barrie, L.A. Biogenic sulfur aerosol in the Arctic troposphere: 1. Contributions to total
764 sulfate. Journal of Geophysical Research: Atmospheres 1993; 98: 20613-20622.
765 https://doi.org/10.1029/93JD02234.
766 Louchouran, P., Kuo, L.-J., Wade, T.L., Schantz, M. Determination of levoglucosan and its
767 isomers in size fractions of aerosol standard reference materials. Atmospheric
768 Environment 2009; 43: 5630-5636. https://doi.org/10.1016/j.atmosenv.2009.07.040.
769 Manousakas, M., Popovicheva, O., Evangeliou, N., Diapouli, E., Sitnikov, N., Shonija, N.,
770 Eleftheriadis, K. Aerosol carbonaceous, elemental and ionic composition variability and
771 origin at the Siberian High Arctic, Cape Baranova. Tellus B: Chemical and Physical
772 Meteorology 2020; 72: 1-14. https://doi.org/10.1080/16000889.2020.1803708.
773 Moffett, C.E., Barrett, T.E., Liu, J., Gunsch, M.J., Upchurch, L., Quinn, P.K., Pratt, K.A.,
774 Sheesley, R.J. Long-term trends for marine sulfur aerosol in the Alaskan Arctic and
775 relationships with temperature. Journal of Geophysical Research: Atmospheres 2020:
776 e2020JD033225. https://doi.org/10.1029/2020JD033225.
777 Moosmüller, H., Chakrabarty, R., Ehlers, K., Arnott, W. Absorption Ångström coefficient,
778 brown carbon, and aerosols: basic concepts, bulk matter, and spherical particles.
779 Atmospheric Chemistry and Physics 2011; 11: 1217-1225. https://doi.org/10.5194/acp-
780 11-1217-2011.

781 Moschos, V., Dzepina, K., Bhattu, D., Lamkaddam, H., Casotto, R., Daellenbach, K.R.,
782 Canonaco, F., Rai, P., Aas, W., Becagli, S., Calzolai, G., Eleftheriadis, K., Moffett, C.E.,
783 Schnelle-Kreis, J., Severi, M., Sharma, S., Skov, H., Vestenius, M., Zhang, W., Hakola,
784 H., Hellén, H., Huang, L., Jaffrezo, J.-L., Massling, A., Nøjgaard, J.K., Petäjä, T.,
785 Popovicheva, O., Sheesley, R.J., Traversi, R., Yttri, K.E., Schmale, J., Prévôt, A.S.H.,
786 Baltensperger, U., El Haddad, I. Equal abundance of summertime natural and wintertime
787 anthropogenic Arctic organic aerosols. Nature Geoscience 2022.
788 https://doi.org/10.1038/s41561-021-00891-1.
789 Popovicheva, O., Diapouli, E., Makshtas, A., Shonija, N., Manousakas, M., Saraga, D., Uttal, T.,
790 Eleftheriadis, K. East Siberian Arctic background and black carbon polluted aerosols at
791 HMO Tiksi. Science of the Total Environment 2019; 655: 924-938.
792 https://doi.org/10.1016/j.scitotenv.2018.11.165.
793 Quinn, P.K., Miller, T., Bates, T.S., Ogren, J., Andrews, E., Shaw, G. A 3-year record of
794 simultaneously measured aerosol chemical and optical properties at Barrow, Alaska.
795 Journal of Geophysical Research: Atmospheres 2002; 107: AAC 8-1-AAC 8-15.
796 https://doi.org/10.1029/2001JD001248.
797 Quinn, P.K., Bates, T.S., Schulz, K., Shaw, G.E. Decadal trends in aerosol chemical composition
798 at Barrow, Alaska: 1976-2008. Atmospheric Chemistry and Physics 2009; 9: 8883-8888.
799 https://doi.org/10.5194/acp-9-8883-2009.
800 Rolph, G., Stein, A., Stunder, B. Real-time environmental applications and display system:
801 Ready. Environmental Modelling & Software 2017; 95: 210-228.
802 https://doi.org/10.1016/j.envsoft.2017.06.025.

803 Russell, L.M., Hawkins, L.N., Frossard, A.A., Quinn, P.K., Bates, T.S. Carbohydrate-like
804 composition of submicron atmospheric particles and their production from ocean bubble
805 bursting. Proceedings of the National Academy of Sciences 2010; 107: 6652-6657.
806 https://doi.org/10.1073/pnas.0908905107.
807 Schmeisser, L., Andrews, E., Ogren, J.A., Sheridan, P., Jefferson, A., Sharma, S., Kim, J.E.,
808 Sherman, J.P., Sorribas, M., Kalapov, I., Arsov, T., Angelov, C., Mayol-Bracero, O.L.,
809 Labuschagne, C., Kim, S-W., Hoffer, A., Lin, N-H., Chia, H-P., Bergin, M., Sun, J., Liu,
810 P., Wu, H. Classifying aerosol type using in situ surface spectral aerosol optical
811 properties. Atmospheric Chemistry and Physics 2017; 17: 12097-12120.
812 https://doi.org/10.5194/acp-17-12097-2017.
813 Schroeder, W., Oliva, P., Giglio, L., Csiszar, I.A. The New VIIRS 375 m active fire detection
814 data product: Algorithm description and initial assessment. Remote Sensing of
815 Environment 2014; 143: 85-96. https://doi.org/10.1016/j.rse.2013.12.008.
816 Sharma, S., Andrews, E., Barrie, L., Ogren, J., Lavoué, D. Variations and sources of the
817 equivalent black carbon in the high Arctic revealed by long-term observations at Alert
818 and Barrow: 1989–2003. Journal of Geophysical Research: Atmospheres 2006; 111.
819 https://doi.org/10.1029/2005JD006581.
820 Sharma, S., Chan, E., Ishizawa, M., Toom-Sauntry, D., Gong, S.L., Li, S.M., Tarasick, D.W.,
821 Leaitch, W.R., Norman, A., Quinn, P.K., Bates, T.S., Levasseur, M., Barrie, L.A.,
822 Maenhaut, W. Influence of transport and ocean ice extent on biogenic aerosol sulfur in
823 the Arctic atmosphere. Journal of Geophysical Research-Atmospheres 2012; 117.
824 https://doi.org/10.1029/2011JD017074.

825 Shaw, P., Russell, L., Jefferson, A., Quinn, P.K. Arctic organic aerosol measurements show
826 particles from mixed combustion in spring haze and from frost flowers in winter.
827 Geophysical Research Letters 2010; 37. https://doi.org/10.1029/2010GL042831.
828 Sheehan, P.E., Bowman, F.M. Estimated effects of temperature on secondary organic aerosol
829 concentrations. Environmental Science & Technology 2001; 35: 2129-2135.
830 https://doi.org/10.1021/es001547g.
831 Shilling, J., and Flynn, C. 2015, updated hourly. Aerosol Optical Properties
832 (AOPCLAP1FLYNN1M). 2016-08-18 to 2017-07-19, North Slope of Alaska (NSA)
833 External Data (satellites and others) (X1). Atmospheric Radiation Measurement (ARM)
834 user facility Data Center: Oak Ridge, Tennessee, USA. Data set accessed 2021-07-01.
835 Shilling, J., and Flynn, C. 2016, updated hourly. Aerosol Optical Properties
836 (AOPPSAP1FLYNN1H). 2017-07-12 to 2017-07-19, ARM Mobile Facility (OLI)
837 Oliktok Point, Alaska; AMF3 (M1). Atmospheric Radiation Measurement (ARM) user
838 facility Data Center: Oak Ridge, Tennessee, USA. Data accessed 2021-07-01.
839 Sinha, P., Kondo, Y., Koike, M., Ogren, J., Jefferson, A., Barrett, T.E., Sheesley, R.J., Ohata, S.,
840 Moteki, N., Coe, H., Liu, D., Irwin, M., Tunved, P., Quinn, P.K., Zhao, Y. Evaluation of
841 ground-based black carbon measurements by filter-based photometers at two Arctic sites.
842 Journal of Geophysical Research: Atmospheres 2017; 122: 3544-3572.
843 https://doi.org/10.1002/2016JD025843.
844 Stein, A., Draxler, R.R., Rolph, G.D., Stunder, B.J., Cohen, M., Ngan, F. NOAA's HYSPLIT
845 atmospheric transport and dispersion modeling system. Bulletin of the American
846 Meteorological Society 2015; 96: 2059-2077. https://doi.org/10.1175/BAMS-D-14-
847 00110.1.

848 Stocker, T. Climate change 2013: the physical science basis: Working Group I contribution to
849 the Fifth assessment report of the Intergovernmental Panel on Climate Change:
850 Cambridge University Press, 2014.
851 Stohl, A., Berg, T., Burkhart, J., Fjæraa, A., Forster, C., Herber, A., Hov, Ø., Lunder, C.,
852 McMillan, W.W., Oltmans, S., Shiobara, M., Simpson, D., Solberg, S., Stebel, K., Ström,
853 J., Tørseth, K., Treffeisen, R., Virkkunen, K., Yttri, K.E. Arctic smoke–record high air
854 pollution levels in the European Arctic due to agricultural fires in Eastern Europe in
855 spring 2006. Atmospheric Chemistry and Physics 2007; 7: 511-534.
856 https://doi.org/10.5194/acp-7-511-2007.
857 Stuiver, M., Polach, H.A. Reporting Of C-14 Data - Discussion. Radiocarbon 1977; 19: 355-363.
858 https://doi.org/10.1017/S0033822200003672.
859 Svendby, T., Lazaridis, M., Tørseth, K. Temperature dependent secondary organic aerosol
860 formation from terpenes and aromatics. Journal of Atmospheric Chemistry 2008; 59: 25-
861 46. https://doi.org/10.1007/s10874-007-9093-7.
862 Walker, D.A., Raynolds, M.K., Daniëls, F.J., Einarsson, E., Elvebakk, A., Gould, W.A., Katenin,
863 A.E., Kholod, S.S., Markon, C.J., Melnikov, E.S., Moskalenko, N.G., Talbot, S.S.,
864 Yurtsev, B.A. The circumpolar Arctic vegetation map. Journal of Vegetation Science
865 2005; 16: 267-282. https://doi.org/10.1111/j.1654-1103.2005.tb02365.x.
866 Williams, K., Jones, A., Roberts, D., Senior, C., Woodage, M. The response of the climate
867 system to the indirect effects of anthropogenic sulfate aerosol. Climate Dynamics 2001;
868 17: 845-856. https://doi.org/10.1007/s003820100150.

869 Willis, M.D., Leaitch, W.R., Abbatt, J.P. Processes controlling the composition and abundance
870 of Arctic aerosol. Reviews of Geophysics 2018; 56: 621-671.
871 https://doi.org/10.1029/2018RG000602.
872 Winiger, P., Barrett, T.E., Sheesley, R.J., Huang, L., Sharma, S., Barrie, L., Yttri, K.E.,
873 Evangeliou, N., Eckhardt, S., Stohl, A., Klimont, Z., Heyes, C., Semiletov, I.P., Dudarev,
874 O.V., Charkin, A., Shakhova, N., Holmstrand, H., Andersson, A., Gustafsson, Ö. Source
875 apportionment of circum-Arctic atmospheric black carbon from isotopes and modeling.
876 Science Advances 2019; 5: eaau8052. https://doi.org/10.1126/sciadv.aau8052.
877 Yamagami, A., Matsueda, M., Tanaka, H.L. Extreme Arctic cyclone in August 2016.
878 Atmospheric Science Letters 2017; 18: 307-314. https://doi.org/10.1002/asl.757.
879 Yoon, S., Ortiz, S.M., Clark, A.E., Barrett, T.E., Usenko, S., Duvall, R.M., Ruiz, L.H., Bean,
880 J.K., Faxon, C.B., Flynn, J.H., Lefer, B.L., Leong, Y.J., Griffin, R.J., Sheesley, R.J.
881 Apportioned primary and secondary organic aerosol during pollution events of
882 DISCOVER-AQ Houston. Atmospheric Environment 2021; 244: 117954.
883 https://doi.org/10.1016/j.atmosenv.2020.117954.
884 Yttri, K.E., Simpson, D., Nøjgaard, J., Kristensen, K., Genberg, J., Strenström, K., Swietlicki, E.,
885 Hillamo, R., Aurela, M., Bauer, H., Offenberg, J.H., Jaoui, M., Dye, C., Eckhardt, S.,
886 Burkhard, J.F., Stoh, A., and Glasius, M. Source apportionment of the summer time
887 carbonaceous aerosol at Nordic rural background sites. Atmospheric Chemistry and
888 Physics 2011; 11: 13339-13357. https://doi.org/10.5194/acp-11-13339-2011.
889 Zhang, J., Ashjian, C., Campbell, R., Hill, V., Spitz, Y.H., Steele, M. The great 2012 Arctic
890 Ocean summer cyclone enhanced biological productivity on the shelves. Journal of

Geophysical Research: Oceans 2014; 119: 297-312. https://doi.org/10.1002/2013JC009301.

Zotter, P., El-Haddad, I., Zhang, Y., Hayes, P.L., Zhang, X., Lin, Y.H., Wacker, L., Schnelle-Kreis, J., Abbaszade, G., Zimmermann, R., Surratt, J.D., Weber, R., Jimenez, J.L., Szidat, S., Baltensperger, U., Prévôt, A.S.H. Diurnal cycle of fossil and nonfossil carbon using radiocarbon analyses during CalNex. Journal of Geophysical Research: Atmospheres 2014; 119: 6818-6835. https://doi.org/10.1002/2013JD021114.

UQK 2015

OLK 2015

Temp. (°C)

OC (ng m^{-3})

EC (ng m^{-3})

UQK 2016

OLK 2016

UQK 2017

OLK 2017

Temperature (°C)

Ambient Conc. (ng m^{-3})

6/01 7/01 8/01 9/01 10/01

Date

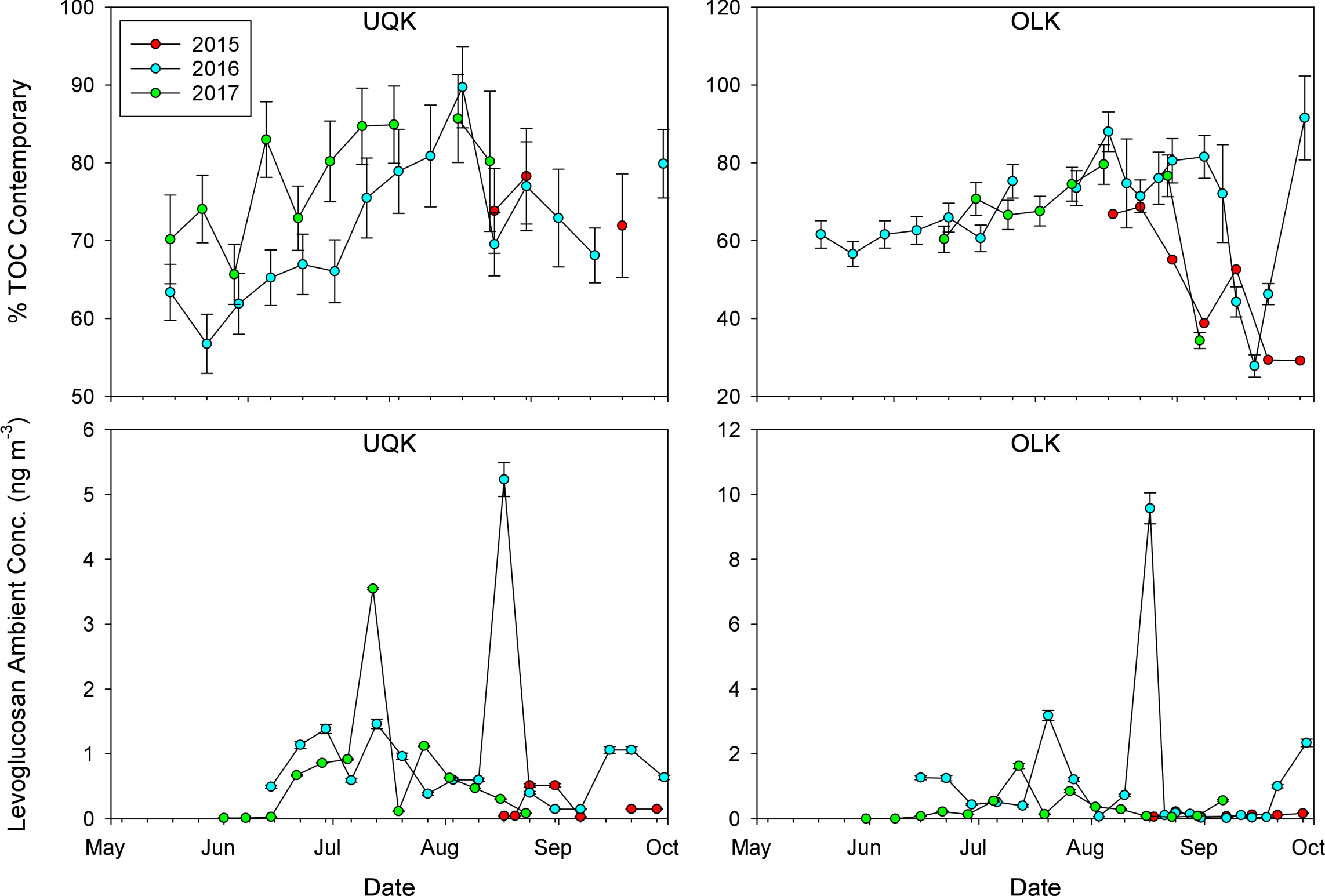
UQK
OLK
2015
2016
2017
% TOC Contemporary
Levoglucosan Ambient Conc. (ng m-3)
Date
May
Jun
Jul
Aug
Sep
Oct

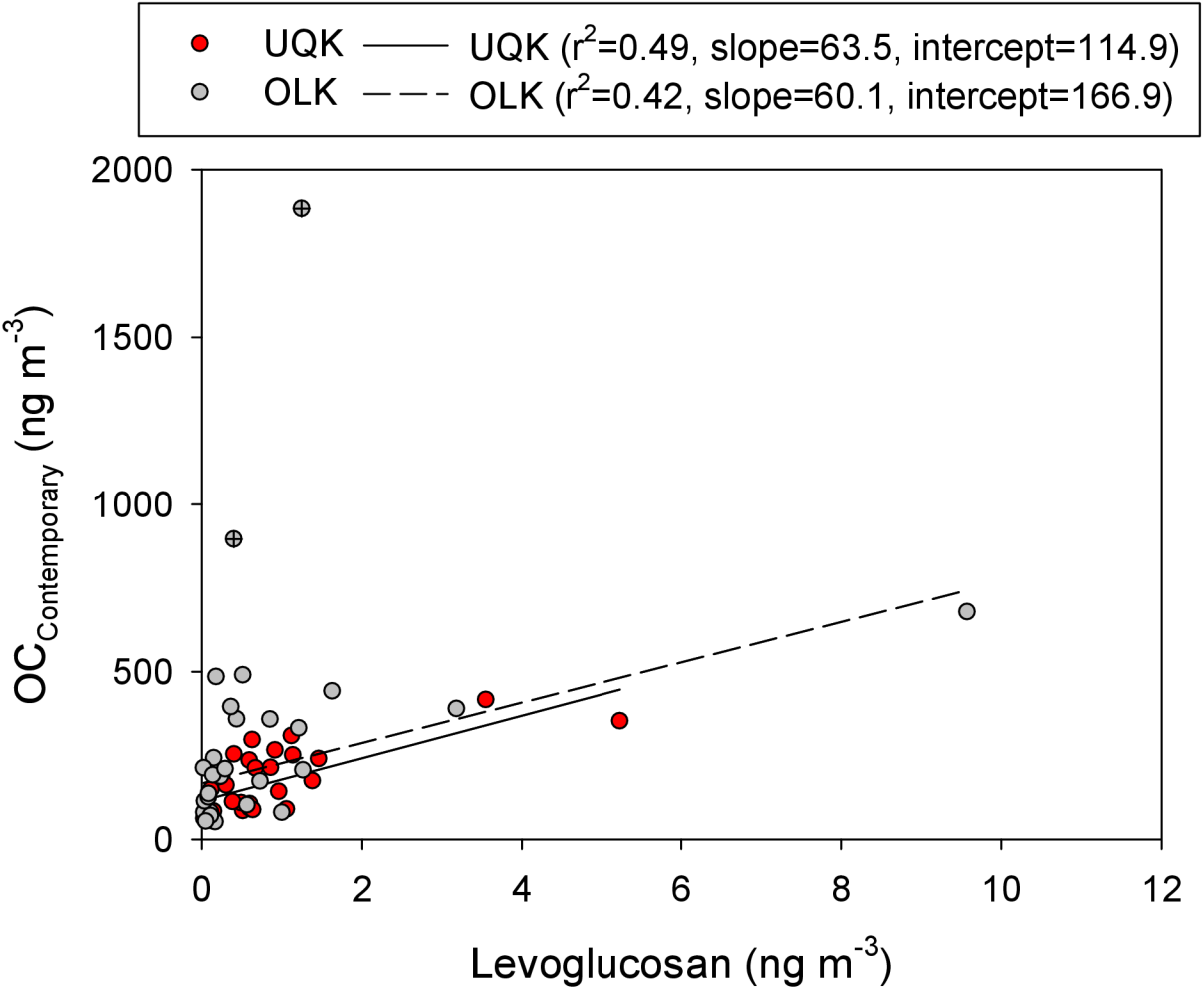
UQK
OLK
UQK (r^2=0.49, slope=63.5, intercept=114.9)
OLK (r^2=0.42, slope=60.1, intercept=166.9)
2000
1500
1000
500
0
0
2
4
6
8
10
12
$OC_{Contemporary}$ (ng m^{-3})
Levoglucosan (ng m^{-3})

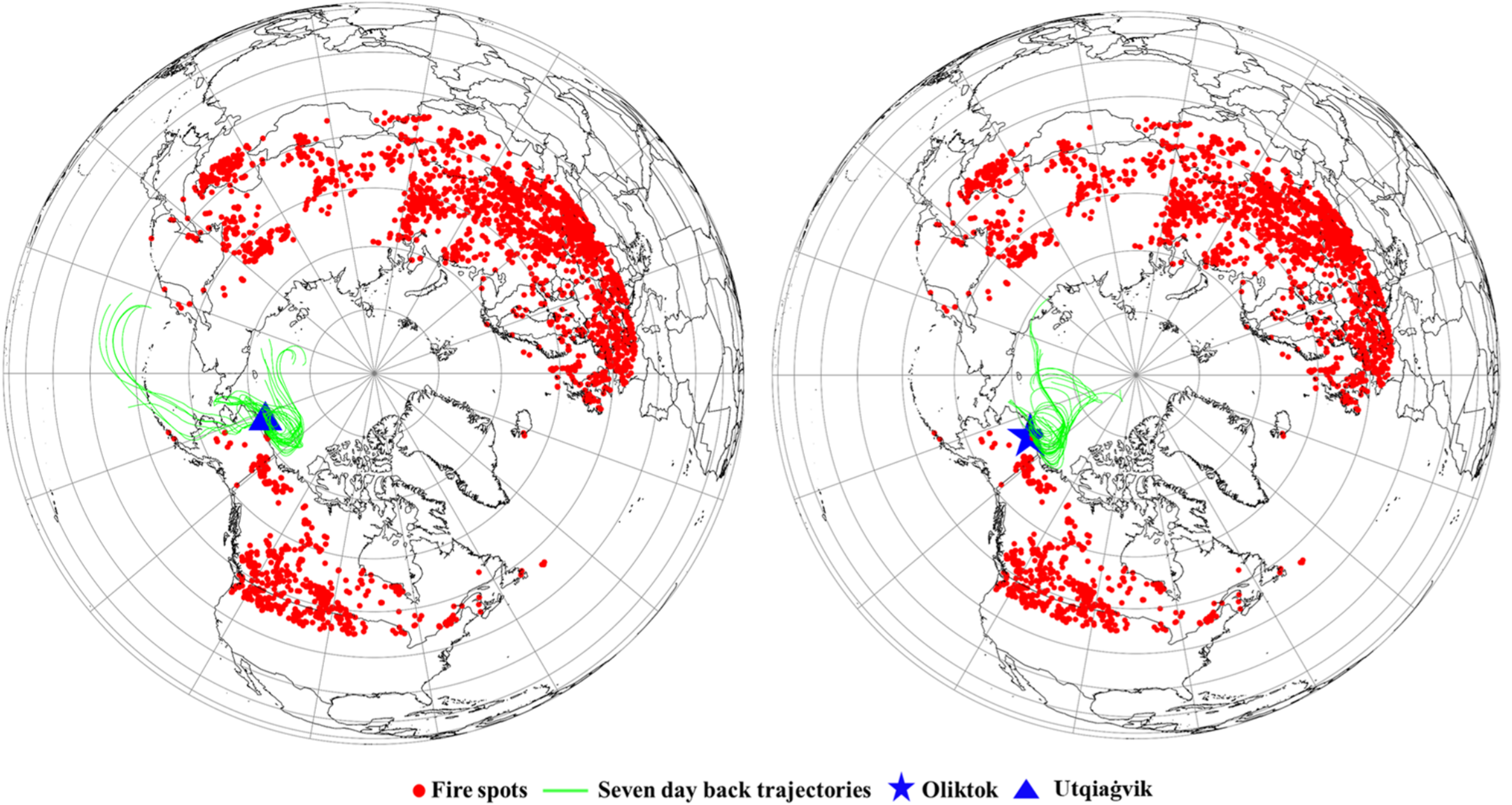
Fire spots
Seven day back trajectories
Oliktok
Utqiaġvik

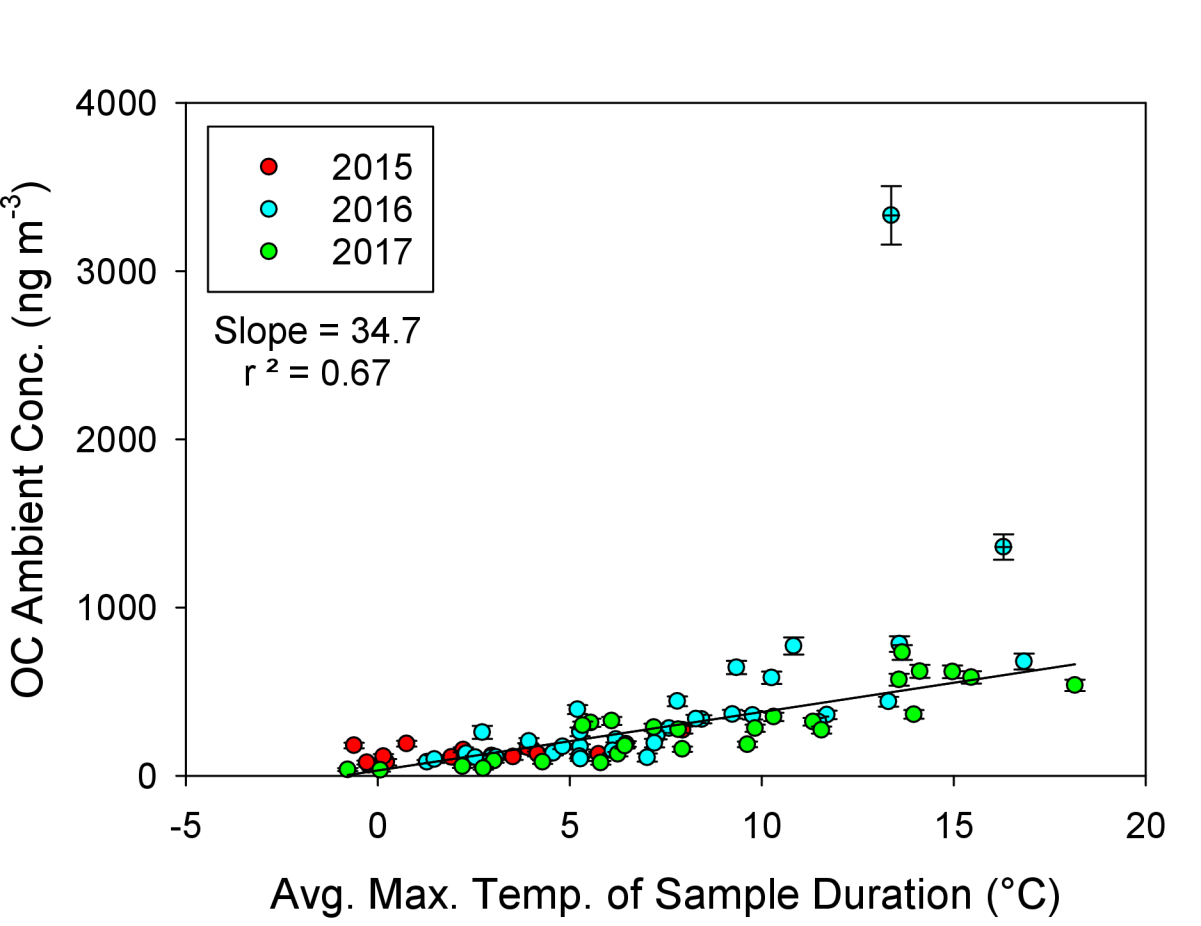
2015
2016
2017
Slope = 34.7
r ² = 0.67
OC Ambient Conc. (ng m-3)
Avg. Max. Temp. of Sample Duration (°C)
4000
3000
2000
1000
0
-5
0
5
10
15
20

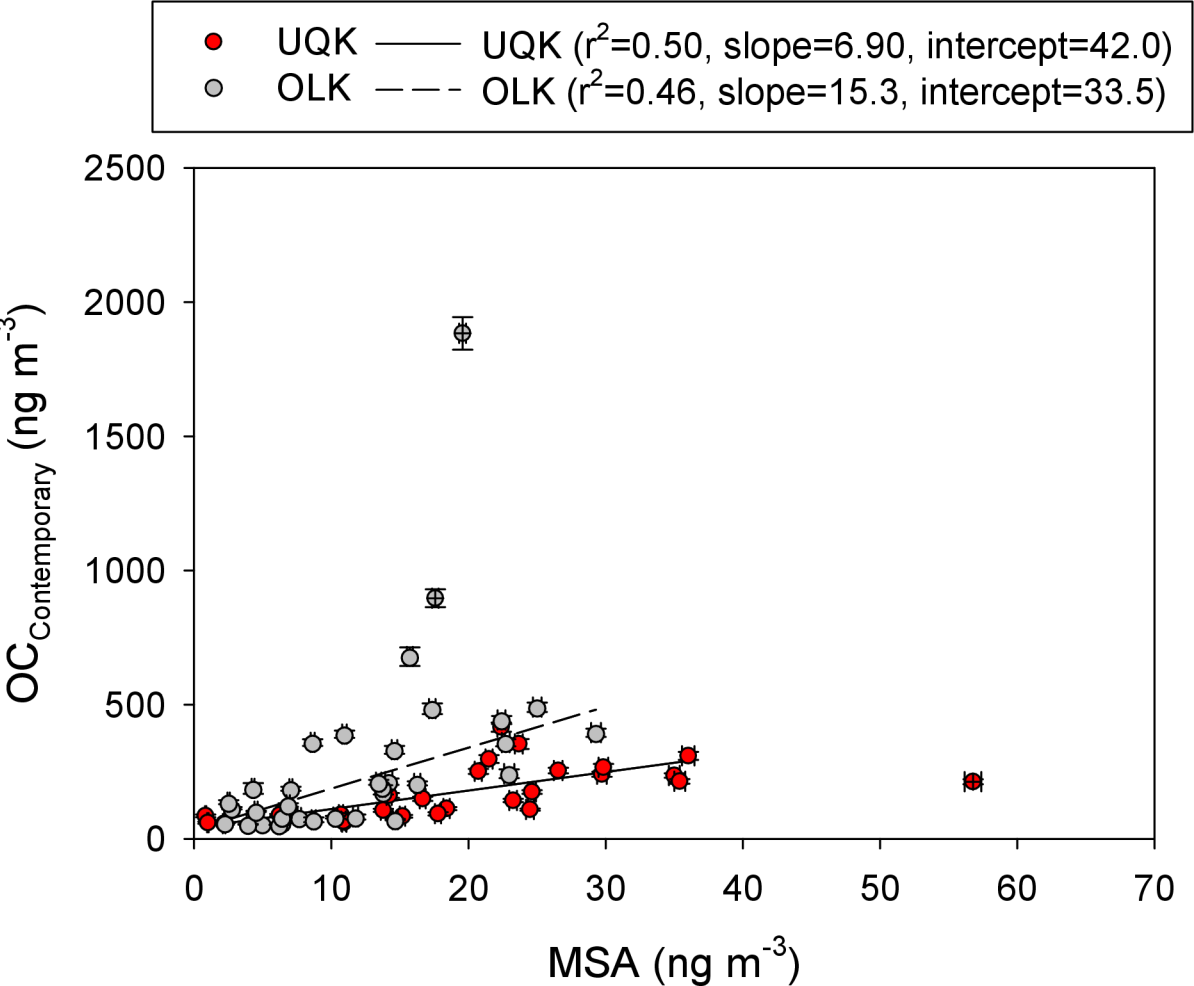
UQK
OLK
UQK (r^2=0.50, slope=6.90, intercept=42.0)
OLK (r^2=0.46, slope=15.3, intercept=33.5)
$OC_{Contemporary}$ (ng m^{-3})
MSA (ng m^{-3})
0
500
1000
1500
2000
2500
0
10
20
30
40
50
60
70

	Utqiaġvik, AK			
Sample Start	8/17/16	9/15/16	9/21/16	**7/12/17**
Sample End	8/24/16	9/21/16	9/30/16	**7/19/17**
Levo Conc. (ng m^{-3})	5.23	0.15	1.06	**3.55**
Levo:OC ratio	0.0133	0.0080	0.0097	**0.0062**
Source Region Identified Using Fire Spot Data	Yes: Russia/Siberia	No	Yes: Russia/Siberia	**Yes: Russia/Siberia, Central Alaska**
HMS Smoke Product Days Available	8/8	7/7	10/10	**7/8**
Number of Days of Smoke Cover	0/8	0/7	0/10	**4/7**
Avg. AAE for Sample Period	0.7 ± 0.4	0.7 ± 0.5	0.7 ± 0.4	**N/A**
Avg. AAE for Summer	0.8 ± 0.4	0.8 ± 0.4	0.8 ± 0.4	**0.79 ± 0.44**
AOD Enhancement	No Data	No Data	No Data	**Yes**

	Oliktok Point, AK					
Sample Start	6/15/16	7/20/16	8/17/16	9/21/16	9/29/16	**7/12/17**
Sample End	6/22/16	7/27/16	8/21/16	9/29/16	10/5/16	**7/19/17**
Levo Conc. (ng m^{-3})	1.27	3.18	9.57	1.00	2.34	**1.63**
Levo:OC ratio	0.0038	0.0049	0.0124	0.0058	0.0114	**0.0005**
Source Region Identified Using Fire Spot Data	Yes: Russia/Siberia	No	Yes: Russia/Siberia	Yes: Russia/Siberia, Aleutian Islands	Yes: Russia/Siberia, Alaska	**Yes: Russia/Siberia**
HMS Smoke Product Days Available	8/8	8/8	8/8	9/9	7/7	**7/8**
Number of Days of Smoke Cover	0/8	0/8	0/8	0/9	0/7	**6/7**
Avg. AAE for Sample Period	N/A	N/A	N/A	N/A	N/A	**1.3 ± 0.4**
Avg. AAE for Summer	N/A	N/A	N/A	N/A	N/A	**1.0 ± 0.4**

AOD Enhancement	No	No	No	No	No	**Yes**

Year	Utqiaġvik, AK				Oliktok Point, AK			
	Avg. Temp. (°C)	Max. Temp. (°C)	Min. Temp. (°C)	r^2 of OC and Avg. Max. Temp.	Avg. Temp. (°C)	Max. Temp. (°C)	Min. Temp. (°C)	r^2 of OC and Avg. Max. Temp.
2015*	1.37	11.2	-7.8	**0.62**	1.43	16.9	-9.9	0.30
2016	2.27	19.1	-4.3	**0.64**	4.35	27.3	-4.7	**0.61**
2017	3.18	21.5	-5.6	**0.75**	4.69	26.7	-4.6	**0.75**
* Only includes temperature data from August and September 2015								

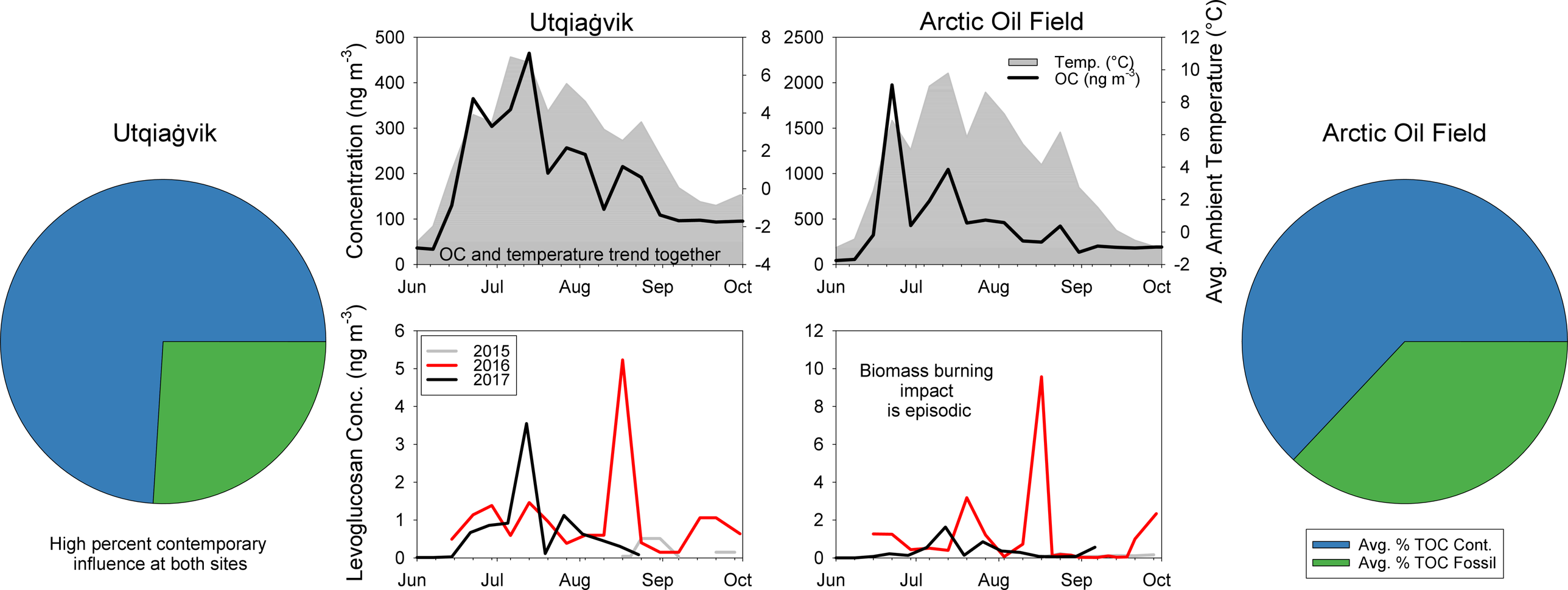
Utqiaġvik
Arctic Oil Field
Concentration (ng m-3)
Avg. Ambient Temperature (°C)
Temp. (°C)
OC (ng m-3)
OC and temperature trend together
Jun
Jul
Aug
Sep
Oct
Levoglucosan Conc. (ng m-3)
2015
2016
2017
Biomass burning
impact
is episodic
Utqiaġvik
High percent contemporary
influence at both sites
Arctic Oil Field
Avg. % TOC Cont.
Avg. % TOC Fossil